STAT1-driven FcRn suppression in macrophages limits antibody protection during bacterial sepsis

Xinyu Wei[1,2]†, Xiaoxia Su[2]†, Qianyu Duan[1]†, Miao Pei[2], Qun Huang[1], Xuan Lai[1], Jiani Zhuang[1], Danzhi Wu[1], Beibei Chen[1], Yu Deng[1], Ying Huang[1], Jinzhou Ye[1], Teng Zhang[1], Hua Zhou[3], Xiaoting Hua[4,5], Xin Ding[6], Mao Li[2,7], Xianjie Liu[8]*, Wenjun Chen[9]*, Xinhai Chen[1,2,10]*

[1]Insititute of Infectious Diseases, Shenzhen Bay Laboratory, Shenzhen 518132, China.

[2]Shenzhen Medical Academy of Research and Translation, Shenzhen 518107, China.

[3]Department of Respiratory and Critical Care Medicine, the Second Affiliated Hospital Zhejiang University, Hangzhou 310009, China.

[4]Department of Infectious Diseases, Sir Run Run Shaw Hospital, Zhejiang University School of Medicine, Hangzhou, 310016, China.

[5]Zhejiang Provincial Engineering Research Center of Innovative Instruments for Precise Pathogen Detection, Hangzhou, 310016, China.

[6]School of Medicine, Shenzhen Campus of Sun Yat-sen University, Shenzhen, 518107, China.

[7]Institute of Chemical Biology, Shenzhen Bay Laboratory, Shenzhen 518132, China.

[8]Shenzhen International Institute for Biomedical Research, Shenzhen 518116, China.

[9]Department of Laboratory Medicine, Third Affiliated Hospital of Sun Yat-Sen University, Tianhe Road 600#, Guangzhou 510630, China.

[10]Guangdong Provincial Key Laboratory of Infection Immunity and Inflammation, Shenzhen 518060, China.

***Corresponding author. Email: xinhaichen@szbl.ac.cn (X.C.); chenwj286@mail.sysu.edu.cn (W.C.); lxj309@163.com (X.L.).**

†These authors contributed equally to this work.

Abstract:

Sepsis is frequently accompanied by reduced circulating IgG levels, but the mechanism and therapeutic implications remain unclear. Here, we show that bacterial sepsis accelerates clearance of both endogenous and therapeutic IgG independently of antigen specificity. Lipopolysaccharide and peptidoglycan activate STAT1 in hepatic and splenic macrophages, leading to selective downregulation of the neonatal Fc receptor (FcRn), impaired IgG recycling, and enhanced intracellular degradation. Macrophage-specific deletion of *Fcgrt* abolishes sepsis-induced IgG loss, whereas genetic or pharmacologic inhibition of STAT1 restores FcRn expression, preserves circulating IgG, and enhances the protective efficacy of intravenous immunoglobulin and pathogen-specific monoclonal antibodies. In human sepsis, reduced FcRn expression in monocytes correlates with poor outcome, and bacterial or PAMP stimulation suppresses FcRn and IgG transcytosis in primary macrophages in a STAT1-dependent manner. These findings identify STAT1-driven suppression of macrophage FcRn as a conserved mechanism limiting antibody protection during bacterial sepsis.

Main Text:

Bacteremia often progresses to sepsis, a life-threatening condition characterized by dysregulated immune responses to invading pathogens. In septic patients, decreased IgG levels are consistently associated with increased mortality [1-3]. Although this correlation is well-established, the mechanism underlying IgG reduction remains elusive. Several hypotheses have been proposed, including antigen-driven consumption, extravasation resulting from increased vascular permeability, B cell dysfunction, and accelerated catabolism [4-6]. However, the relative contributions of these processes remain poorly defined, and the potential involvement of other, unrecognized mechanisms cannot be ruled out. Elucidating these mechanisms are therefore critical for developing novel therapeutic strategies for bacterial sepsis.

Driven by the antibiotic resistance crisis, antibody therapies have been developed for bacterial sepsis, yet the majority of their clinical trials have failed for reasons that are still poorly understood [7,8]. The observed reduction in endogenous IgG levels during sepsis raises the possibility that a parallel reduction may occur in the circulating concentrations of exogenously administered therapeutic antibodies. This could explain the inconsistent clinical outcomes reported with intravenous immunoglobulin (IVIG) in septic patients [5,9]. If a general mechanism driving IgG reduction exists, it also likely compromises the pharmacokinetics of pathogen-specific antibodies, preventing them from reaching and maintaining therapeutic levels. This may account for the heterogeneous efficacy observed in clinical evaluations of those antibody therapies.

IgG antibodies can clear bacterial infections via FcγR- and complement receptor (CR)-mediated phagocytosis, leading to lysosomal degradation of both the antibodies and engulfed pathogens [10,11]. In parallel, the neonatal Fc receptor (FcRn) critically influences IgG homeostasis by orchestrating

a salvage pathway that recycles IgG from lysosomal degradation, thereby ensuring its prolonged circulating half-life [12]. At present, it remains unclear whether sepsis alters the function of these receptors and whether such impairment ultimately contributes to a characteristic decline in circulating antibody levels. Defining the dominant mechanism and identifying key therapeutic targets are crucial for rescuing antibody efficacy in sepsis.

Results

Mouse sepsis recapitulates circulating IgG loss observed in patients

Profiling of patients with bacterial sepsis stratified by survival outcome revealed a striking divergence in endogenous IgG kinetics (Fig. 1A). Specifically, survivors exhibited a fluctuating rise in IgG levels over time, in contrast to the overall stagnation or decline observed in non-survivors, a finding with significant prognostic implications. Intriguingly, a similar decline in endogenous total IgG levels was also observed in mouse models of sepsis induced by bloodstream infection with either pathogenic *Escherichia coli* (Gram-negative bacterium) or a *Staphylococcus aureus* (Gram-positive bacterium) strain deficient in *spa*, *sbi*, and *ssl10* genes (Fig. 1B; fig. S1, A and B). These genes encode immunoglobulin-binding proteins previously shown in our work to mediate circulating IgG loss [13], a process that could confound the sepsis-specific phenotype under investigation. While endogenous total IgM levels also decreased in these mouse sepsis models (Fig. 1C), administration of intravenous immunoglobulin (IVIG), which contains both human IgG (hIgG) and IgM (hIgM), revealed a critical divergence in clearance kinetics between IgG and IgM (Fig. 1, D and E). Specifically, bacterial sepsis markedly accelerated the clearance of hIgG but left hIgM clearance unchanged. To substantiate this finding, we tracked the clearance of exogenous IgG monoclonal antibodies (mAbs) that were not specific to the infecting pathogens (Fig. 1, F-J). These included a hIgG1 administered to both wild-type (WT) and mature B cell-deficient (DKO)

mice, a long-acting hIgG1 variant with YTE mutations [14,15] evaluated in human FcRn (hFcRn) transgenic mice, and a mouse IgG2b (mIgG2b). All of these exogenous IgG forms exhibited more rapid decline during sepsis (Fig. 1, F-J). In contrast, a mIgM mAb recognizing the same antigen as the mIgG2b did not show accelerated clearance (Fig. 1K). This dissociation suggests that distinct mechanisms underlie the loss of endogenous IgG versus IgM, with the former potentially sharing a common pathway with accelerated clearance of exogenous IgG.

To determine the mechanism underlying this accelerated IgG clearance, we first investigated whether it could be attributed to enhanced tissue distribution or fecal excretion. However, the hIgG1 levels in both perfused and non-perfused tissues, as well as fecal samples, did not differ significantly between septic and control mice (Fig. 1, L-N). Furthermore, the clearance mechanism was independent of antigen recognition. This was evidenced by the fact that the IVIG preparation contained negligible pathogen-specific antibodies (fig. S1, C and D), all administered mAbs were non-binding to the pathogens used (fig. S1, E and F), and no anti-*E. coli* or anti-*S. aureus* antibodies were detectable in the serum of septic mice during the experimental timeframe (fig. S1, G-J). Together, these results strongly support that bacterial sepsis drives the loss of both endogenous and exogenous IgG in mice through a mechanism consistent with non-antigen-specific consumption.

Macrophage FcRn reduction mediates circulating IgG loss in septic mice

Having ruled out non-specific consumption, we hypothesized that the accelerated IgG clearance was mediated by receptors governing IgG homeostasis. To this end, we primarily profiled the expression of FcγRs, CRs, and FcRn in immune cells from septic mice, including neutrophils, monocytes, and macrophages in both circulation and tissues, by flow cytometry. However, our

screening revealed that the expression changes of individual FcγRs and CRs lacked a consistent or unified trend between the *E. coli* and *S. aureus* sepsis models (fig. S2), arguing against their primary role in the observed IgG loss. Strikingly, we discovered a convergent downregulation of FcRn in liver and splenic macrophages across both bacterial sepsis models (Fig. 2, A and B; fig. S3A), which was further confirmed at the transcriptional level (fig. S3B), although the abundance of hepatic macrophages (Kupffer cells) was not markedly reduced (fig. S3, C and D). Given the established role of endothelial FcRn in IgG homeostasis [12], we extended our analysis to liver and lung endothelial cells. Although we observed a moderate reduction in endothelial cell numbers in liver (fig. S3, E-H), FcRn expression in these cells was not significantly altered (Fig. 2, A and B). To establish a direct causal link, we employed an *in vitro* model using bone marrow-derived macrophages (BMDMs). Bacterial challenge recapitulated the *in vivo* findings, inducing significant downregulation of FcRn at both the protein and transcriptional levels (Fig. 2, C and D). To determine if the observed FcRn downregulation directly mediates circulating IgG loss, we subjected *Fcgrt*$^{-/-}$ mice to our established bacterial sepsis models (fig. S3, I and J). Upon infection with either pathogenic *E. coli* or *S. aureus*, both WT and *Fcgrt*$^{-/-}$ mice exhibited comparable body weight loss and bacterial loads across tissues (fig. S3, K-N), indicating a similar disease severity. Strikingly, unlike in WT mice, endogenous IgG levels in *Fcgrt*$^{-/-}$ mice did not decline significantly in response to sepsis (Fig. 2E and 1B). Similarly, the clearance of administered hIgG1 was not accelerated in septic *Fcgrt*$^{-/-}$ mice compared to their non-septic counterparts (Fig. 2F and 1F). To further define the role of macrophage FcRn, we generated mice with a myeloid-specific knockout of *Fcgrt* (*Fcgrt*$^{f/f}$ *LysM-Cre*). Bacterial sepsis induced by either pathogen resulted in body weight loss and tissue bacterial loads that were indistinguishable between *Fcgrt*$^{f/f}$ and *Fcgrt*$^{f/f}$ *LysM-Cre* mice (Fig. 2, G-I), ruling out confounding differences in infection dynamics. Notably, the accelerated IgG clearance found in septic *Fcgrt*$^{f/f}$ controls was absent in septic *Fcgrt*$^{f/f}$ *LysM-Cre*

mice (Fig. 2, J and K), indicating that the sepsis-induced downregulation of FcRn in macrophages is a primary driver of the circulating IgG decline.

LPS and PGN reduce macrophage FcRn, leading to circulating IgG loss

We next asked which bacterial components trigger the FcRn-dependent IgG loss. Given the established role of LPS as a key mediator in sepsis, we first employed toll-like receptor 4 (TLR4)-deficient mice subjected to pathogenic *E. coli*-induced sepsis. The accelerated decline in hIgG1 levels observed in $TLR4^{+/+}$ control mice was absent in $TLR4^{-/-}$ mice (Fig. 3A), despite equivalent disease severity as measured by body weight loss and tissue bacterial loads (fig. S4, A and B), indicating that the phenotype was not attributable to differences in infection outcome. Since LPS is essential in *E. coli*, we utilized *Acinetobacter baumannii*, employing both WT and an LPS-deficient mutant strain with a IS*Aba1* insertion in *lpxC* [16] (Fig. 3, B and C). Although LPS loss markedly attenuates virulence [17], to compensate for this, we administered a threefold higher inoculum of the mutant strain. This achieved comparable bacterial loads across tissues between mutant- and WT-infected mice at 6-24 hours post-infection (fig. S4C). Using this model, we found that only WT *A. baumannii* infection reduced endogenous IgG levels and accelerated the clearance of exogenous hIgG1 (Fig. 3, B and C). Despite similar bacterial loads during early infection, the LPS-deficient mutant did not recapitulate the IgG loss phenotype (Fig. 3, B and C), demonstrating that LPS is the principal factor mediating circulating IgG loss in Gram-negative bacteria-induced sepsis. Accordingly, administration of exogenous LPS nearly phenocopied the loss of both endogenous IgG and various exogenous IgG mAbs observed in pathogenic *E. coli* infection (Fig. 3, D-F; Fig. 1, B, F, G, and I), and this effect was also abolished in $TLR4^{-/-}$ mice (Fig. 3G). Similarly, administration of peptidoglycan (PGN) from *S. aureus* induced an acceleration of hIgG1 clearance comparable to that detected in LPS-treated mice (Fig. 3D).

The observed circulating IgG loss mediated by LPS or PGN prompted us to investigate their effect on FcRn expression. *In vivo*, both LPS and PGN selectively downregulated FcRn at the protein and transcriptional levels in splenic and hepatic macrophages (Fig. 3, H and I; fig. S4F), without affecting other tested cells (fig. S4, D and E). The decline in FcRn in splenic macrophages was accompanied by elevated cytokine expression (fig. S4, G and H). This FcRn downregulation was also replicated in BMDMs but not in human umbilical vein endothelial cells (HUVECs) (Fig. 3, J and K; fig. S4, I-K), where robust cytokine induction confirmed effective LPS or PGN treatment (fig. S4, L-N). FcRn deficiency had no impact on the phagocytic capacity of BMDMs with or without LPS stimulation (Fig. 3L). However, intracellular levels of hIgG1 were substantially lower in *Fcgrt*$^{-/-}$ BMDM compared to WT controls (Fig. 3M), indicating rapid IgG degradation in the absence of FcRn. Moreover, LPS and PGN stimulation markedly reduced hIgG1 levels in WT BMDMs (Fig. 3, M and N), directly linking PAMP-induced FcRn downregulation to impaired IgG transcytosis and enhanced intracellular IgG degradation in macrophages. As expected, neither LPS nor PGN alone accelerated the clearance of exogenous hIgG1 in *Fcgrt*$^{-/-}$ mice (Fig. 3, O and P). Collectively, these results indicate that specific bacterial PAMPs, notably LPS and PGN, serve as critical bacterial factors in sepsis-induced circulating IgG loss, operating through selective downregulation of FcRn in macrophages and consequent disruption of IgG homeostasis.

STAT1 activation impairs macrophage FcRn expression in sepsis

We further asked how specific PAMPs during bacterial sepsis reduced FcRn expression in macrophages. Given that LPS or PGN treatment in BMDMs recapitulated the FcRn reduction observed in splenic and liver macrophages during bacterial sepsis (Fig. 2, A and B; Fig. 3, J and K), we first investigated whether NF-κB mediated this reduction in this model. Although NF-κB

is a well-known sepsis-related transcription factor, its inhibition unexpectedly further decreased FcRn expression in LPS- or PGN-treated BMDMs (Fig. 4A), even though it effectively suppressing cytokine expression (fig. S5, A and B). This indicates that NF-κB activation indeed exerts a protective effect on FcRn expression. We next examined the role of type I interferon in FcRn reduction following observations of its robust induction in PAMP- or bacteria-treated macrophages [18] (fig. S5B and S4H). However, in BMDMs from A129 mice (*Ifnar1* knockout), LPS stimulation, while still inducing robust expression of cytokines (fig. S5, C and D), failed to restore FcRn expression (Fig. 4B). Moreover, both bacterial sepsis and LPS administration still accelerated the clearance of hIgG1 in A129 mice (Fig. 4, C and D), mirroring the trend observed in WT mice (Fig. 1F and 3D). A129 mice also exhibited a susceptibility to bacterial sepsis comparable to that of WT mice (fig. S5E). These results indicate that type I interferon is not required for FcRn reduction during sepsis.

To uncover the mechanism underlying FcRn reduction, we performed bulk RNA-seq on Kupffer cells and splenic macrophages isolated from septic mice. Principal component analysis revealed a clear separation between the transcriptomic profiles of Kupffer cells and splenic macrophages from healthy mice and those with bacterial sepsis (Fig. 4E). This transcriptomic data further confirmed that FcRn expression was significantly reduced in both Kupffer cells and splenic macrophages of septic mice (fig. S5F). A total of 503 genes were commonly differentially expressed in these two macrophage populations following bacterial sepsis (Fig. 4F). Using these shared differentially expressed genes for transcription factor (TF) activity inference, we identified 11 TFs whose activities were significantly and concordantly regulated in both Kupffer cells and splenic macrophages during bacterial sepsis (Fig. 4, G and H). Interestingly, two of these TFs, *Stat1* and *Spi1*, were also identified in the public macrophage cistrome data (The Signaling

Pathways Project) as potential direct regulators of the *Fcgrt* locus (Fig. 4H). Treatment with the STAT1 inhibitor fludarabine but not PU.1 (encoded by *Spi1*) inhibitor DB2313 rescued FcRn expression in LPS- or PGN-stimulated BMDMs without suppressing the expression of cytokines (Fig. 4I, fig. S5, G-I). STAT1 has been implicated as a negative regulator for FcRn in response to type II interferon (IFN-γ) *in vitro* [19]; however, its role in regulating FcRn expression during bacterial sepsis remains unclear. We confirmed that bacterial infections or PAMP stimulations markedly induced STAT1 phosphorylation at both tyrosine 701 and serine 727 residues in BMDMs, while failing to trigger IFN-γ expression (Fig. 4J; fig. S5, J and K). To validate this *in vivo*, the *stat1*$^{-/-}$ mice were chosen. Since *stat1*$^{+/+}$ and *stat1*$^{+/-}$ showed a similar trend of accelerated hIgG1 clearance (fig. S5L), we randomly selected one of these two genotypes to serve as the control group in subsequent studies. The *stat1*$^{-/-}$ mice did not exhibit increased susceptibility to bacterial sepsis, as evidenced by comparable body weight loss and tissue bacterial loads to controls (fig. S5, M-O). Strikingly, genetic deletion of *stat1* profoundly rescued FcRn reduction in liver macrophages and significantly, albeit partially, restored FcRn expression in splenic macrophages following bacterial sepsis (Fig. 4, K-N). Consequently, the bacterial sepsis-induced loss of circulating hIgG1 was also significantly ameliorated in *stat1*$^{-/-}$ mice (Fig. 4, O and P). Thus, these data establish STAT1 activation as a pathophysiological promoter of FcRn reduction and resultant circulating IgG loss during bacterial sepsis.

Bacterial infections disrupt IgG transcytosis in human macrophages

We established that in murine bacterial sepsis, bacterial PAMPs activate STAT1 in macrophages, leading to FcRn suppression and loss of circulating IgG. This discovery prompted us to investigate the translational relevance of this modulation in human sepsis. We began by interrogating public datasets to determine whether *Fcgrt* expression is altered in septic patients. Re-analysis of two

independent cohorts confirmed that *Fcgrt* expression was significantly downregulated in whole blood or peripheral leukocytes from septic patients compared to healthy controls (Fig. 5A and fig. S6A). In the GSE65682 dataset, Kaplan-Meier survival analysis with the log-rank test revealed that septic patients with higher *Fcgrt* expression had a greater probability of survival relative to those with lower expression (Fig. 5B). Re-analysis of GSE63042 dataset showed that sepsis survivors exhibited elevated *Fcgrt* levels in whole blood and contained a higher proportion of individuals with high *Fcgrt* expression compared to sepsis non-survivors (Fig. 5, C and D). To validate these findings, we collected blood samples from septic patients and healthy donors. Our analysis of $CD14^+$ monocytes from these samples revealed a significant reduction in FcRn expression in patients (Fig. 5E). We next infected $CD14^+$ monocyte-derived macrophages (hMDMs) with *E. coli* or *S. aureus* and found that this infection triggered a time- and dose-dependent suppression of FcRn expression (Fig. 5, F and G; fig. S6, B and C), a result that consistent with reanalyzed data from public datasets on PBMCs or human macrophages (fig. S6, D and E). Furthermore, our experiments established that LPS or PGN stimulation was sufficient to significantly downregulate FcRn in $CD14^+$ hMDMs (Fig. 5, H and I), an effect we also confirmed in $CD14^+$ monocytes following PAMP challenge (fig. S6, F-J).

We next examined STAT1 signaling pathway. In $CD14^+$ hMDMs, both bacterial infection and PAMP stimulation promptly induced phosphorylation of STAT1 at Ser727 and Tyr701 (Fig. 5, J and K). These phosphorylation events occurred early after exposure, aligning with previous observations in mouse BMDMs (Fig. 4J). The inhibition of STAT1 phosphorylation at Tyr701 (by Ruxolitinib, RUX) or at Ser727 (by Adezmapimod, ADE) in hMDMs rescued the downregulation of FcRn expression induced by LPS or PGN (Fig. 5, L and M), demonstrating STAT1-dependent regulation of FcRn. PAMP stimulation did not reduce the phagocytic capacity of hMDMs (Fig.

5N) but instead reduced their hIgG1 transcytosis (Fig. 5O). Hence, our data demonstrate that in human macrophages, bacteria and their PAMPs activate STAT1 to suppress FcRn, thereby impairing IgG transcytosis. These findings indicate that STAT1-dependent FcRn suppression in macrophages is conserved between mice and humans.

Targeting STAT1-dependent FcRn suppression rescues antibody efficacy in bacterial sepsis

The therapeutic efficacy of antibodies is known to correlate positively with concentration within a defined therapeutic range. Our data are consistent with this principle that IVIG protects against *E. coli* and *S. aureus* sepsis in a clear dose-dependent manner (fig. S7, A and B). To determine whether IVIG efficacy depends on macrophage FcRn expression, we compared outcomes in *Fcgrt*$^{f/f}$ and *Fcgrt*$^{f/f}$ LysM-Cre mice during bacterial sepsis. While macrophage-specific FcRn deletion did not alter host susceptibility to either *E. coli* or *S. aureus* sepsis, it completely abrogated the protective effect of IVIG (Fig. 6, A and B). Specifically, IVIG significantly improved survival in *Fcgrt*$^{f/f}$ mice but failed to protect *Fcgrt*$^{f/f}$ LysM-Cre mice (Fig. 6, A and B), indicating that the loss of IVIG efficacy upon macrophage FcRn deletion is attributable to impaired antibody persistence *in vivo*. Next, we asked whether therapeutic targeting STAT1 signaling could enhance antibody-mediated protection against bacterial sepsis. Notably, genetic ablation of STAT1 did not affect survival in *E. coli* sepsis but slightly increased tolerance to *S. aureus* infection (Fig. 6, C and D). More importantly, IVIG-mediated protection was significantly augmented in *STAT1*$^{-/-}$ mice against both pathogens compared to *STAT1*$^{+/-}$ controls (Fig. 6, C and D). Pharmacologic inhibition of STAT1 with carnosic acid (CA) similarly improved IVIG efficacy (Fig. 6E), confirming that dampening STAT1 activity improves antibody-based intervention outcomes in bacterial sepsis. We extended these findings to a pathogen-specific mAb, 3E9, which targets the conserved O25b LPS antigen of *E. coli* ST131 lineage [20]. Although 3E9 exhibited strong binding to *E. coli* used in

this study (fig. S7C), its low dose provided no protection in WT mice during *E. coli* sepsis (Fig. 6F). In contrast, its efficacy was markedly enhanced in TLR4-deficient mice (Fig. 6F), accompanied by significantly improved serum 3E9 persistence compared to septic $TLR4^{+/+}$ controls (Fig. 6G). Consistently, 3E9 improved survival in $Fcgrt^{f/f}$ mice but failed to protect $Fcgrt^{f/f}$ LysM-Cre mice (Fig. 6H). Furthermore, 3E9 conferred protection in $STAT1^{-/-}$ but not $STAT1^{+/-}$ mice (Fig. 6I). These results demonstrate that interrupting STAT1-dependent FcRn suppression rescues sepsis-induced antibody failure and enhances antibody-mediated protection.

Discussion

Antibodies are essential for defense against bacterial infections, a function that depends on sustained IgG levels to enable rapid responses to pathogenic challenge. However, bacterial sepsis disrupts this fundamental requirement. We found that bacterial sepsis subverts this defense by reducing both endogenous and exogenous IgG in mice, mirroring the clinical observation of decreased circulating IgG in septic patients, where higher levels are associated with improved survival [1-4,21]. Mechanistically, this IgG loss was uncoupled from an antigen-specific immune response, tissue redistribution, or fecal excretion, and was instead mediated by STAT1-dependent suppression of FcRn in macrophages. During sepsis, bacterial components such as LPS and PGN activated STAT1 signaling, leading to suppressed FcRn expression, impaired IgG recycling, and consequently, lowered circulating IgG. Importantly, blocking STAT1 signaling restored antibody protection during sepsis. Our work identifies STAT1-driven FcRn suppression in macrophages as a central mechanism driving antibody loss in bacterial sepsis, providing a conceptual framework and proof-of-principle for targeting this pathway to rescue antibody immunity in septic patients.

While FcRn is widely expressed, its role in maintaining IgG levels is primarily mediated by endothelial cells, macrophages, and monocytes [12,22]. In murine bacterial sepsis, we found that FcRn was specifically downregulated in hepatic and splenic macrophages, which represent over 35% of the total macrophage population [23], while its expression remained unchanged in monocytes and endothelial cells. Importantly, bacterial infection induced a pronounced reduction in liver endothelial cell numbers while sparing the macrophage population; yet, IgG transcytosis was specifically suppressed in macrophages. Since macrophages primarily degrade IgG when FcRn is compromised [24], our observations reveal a critical functional dilemma wherein macrophages face an increased burden of IgG salvage due to the loss of endothelial cells, but simultaneously, their capacity to perform this task is compromised by FcRn downregulation, thereby resulting in IgG hypercatabolism. Thus, FcRn downregulation in splenic and hepatic macrophages constitutes a key mechanism underlying sepsis-induced circulating IgG loss, as evidenced by the fact that *Fcgrt*$^{f/f}$ *LysM-Cre* mice with bacterial sepsis exhibited equivalent levels of IgG loss as those without infection, thereby establishing the central role of macrophages and revealing a previously unrecognized pathogen-induced antibody evasion strategy via FcRn reprogramming.

Although significant interest has focused on FcRn-based therapeutic strategies, the regulation of its expression remains far less explored. If FcRn expression is compromised during infection, then engineering antibody-FcRn affinity alone may be insufficient to achieve the desired therapeutic outcomes. Several viruses have been reported to hijack FcRn. Enterovirus B and human astrovirus utilize FcRn as a functional receptor to facilitate viral replication [25-27]. Human cytomegalovirus employs the US11 protein to bind FcRn and promote its ubiquitin-mediated degradation [28]. Herpes simplex virus-1 infection upregulates DNA methylation at the FCGRT locus to suppress FcRn expression [29]. In contrast, how bacterial infection regulates host FcRn expression has remained

largely undefined. This study identifies that in bacterial sepsis, bacterial LPS and PGN downregulate macrophage FcRn through STAT1 activation. Unlike the previously reported IFN-γ-dependent STAT1-FcRn pathway observed *in vitro* [19], the current findings establish that LPS and PGN directly activate STAT1 in macrophages without substantial IFN-γ induction. This FcRn suppression exhibited striking tissue specificity, occurring specifically in hepatic and splenic macrophages. Thus, our finding, taken together with established tissue-specific methylation patterns at the FCGRT locus [30], suggests distinct regulatory mechanisms for FcRn expression in macrophages, monocytes, and endothelial cells across different tissues. The identification of STAT1-dependent regulation of FcRn provides a compelling rationale for this paradigm, underscoring the critical need to understand pathologic regulation of FcRn for future therapeutic development.

Current management of bacterial sepsis remains centered on infection control and supportive care [31]. Antibody-based therapeutic strategies have long attracted significant attention for their potential to improve outcomes, but none have yet achieved clinical success [32-34]. Such strategies encompass agents ranging from IVIG to mAbs targeting host factors like CD14 or TNFα or specific pathogen-derived antigens. Nevertheless, several antibody-based agents continue to be evaluated in active clinical trials, with many focusing on modulation of host immune responses [35-37]. This collective effort suggests that immunomodulation may offer wide-ranging benefits in septic patients [38,39]. We identify STAT1-driven suppression of FcRn in macrophages as a conserved pathway that limits antibody persistence and protection during bacterial sepsis. Reduced FcRn expression in circulating monocytes of septic patients and its association with survival further support the clinical relevance of this mechanism. In preclinical models, various interventions along this pathway, such as TLR4 knockout and STAT1 deletion or functional inhibition, consistently

improved the protective efficacy of both IVIG and the anti-*E. coli* mAb 3E9 [20] in septic models, whereas macrophage-specific *Fcgrt* knockout abolished that protection. A future refined strategy would be to deliver FcRn mRNA via lipid-based nanoparticles or macrophage-derived exosomes [40-42], thereby enhancing FcRn expression in macrophages and boosting antibody efficacy. Collectively, our work supports the idea that modulating STAT1-dependent FcRn regulation may represent a strategy to improve the performance of antibody-based therapies in bacterial sepsis.

References

1 Bermejo‐Martín, J. F. *et al.* Immunoglobulins IgG1, IgM and IgA: a synergistic team influencing survival in sepsis. *Journal of Internal Medicine* **276**, 404–412 (2014). https://doi.org/10.1111/joim.12265

2 Akatsuka, M., Tatsumi, H., Sonoda, T. & Masuda, Y. Low immunoglobulin G level is associated with poor outcomes in patients with sepsis and septic shock. *Journal of Microbiology, Immunology and Infection* **54**, 728–732 (2021). https://doi.org/10.1016/j.jmii.2020.08.013

3 Taccone, F. S., Stordeur, P., De Backer, D., Creteur, J. & Vincent, J.-L. γ-Globulin Levels in Patients with Community-Acquired Septic Shock. *Shock* **32**, 379–385 (2009). https://doi.org/10.1097/SHK.0b013e3181a2c0b2

4 Venet, F. *et al.* Assessment of plasmatic immunoglobulin G, A and M levels in septic shock patients. *International Immunopharmacology* **11**, 2086–2090 (2011). https://doi.org/10.1016/j.intimp.2011.08.024

5 Akatsuka, M., Masuda, Y., Tatsumi, H. & Sonoda, T. Efficacy of Intravenous Immunoglobulin Therapy for Patients With Sepsis and Low Immunoglobulin G Levels: A Single-Center Retrospective Study. *Clinical Therapeutics* **44**, 295–303 (2022). https://doi.org/10.1016/j.clinthera.2021.12.008

6 Schmidt, C., Weißmüller, S. & Heinz, C. C. Multifaceted Tissue-Protective Functions of Polyvalent Immunoglobulin Preparations in Severe Infections—Interactions with Neutrophils, Complement, and Coagulation Pathways. *Biomedicines* **11** (2023). https://doi.org/10.3390/biomedicines11113022

7 Chen, X. & Missiakas, D. Novel Antibody-Based Protection/Therapeutics in Staphylococcus aureus. *Annual Review of Microbiology* **78**, 425–446 (2024). https://doi.org/10.1146/annurev-micro-041222-024605

8 Wang, H., Chen, D. & Lu, H. Anti-bacterial monoclonal antibodies: next generation therapy against superbugs. *Applied Microbiology and Biotechnology* **106**, 3957–3972 (2022). https://doi.org/10.1007/s00253-022-11989-w

9 Tagami, T., Matsui, H., Fushimi, K. & Yasunaga, H. Intravenous Immunoglobulin and Mortality in Pneumonia Patients With Septic Shock: An Observational Nationwide

Study. *Clinical Infectious Diseases* **61**, 385–392 (2015). https://doi.org/10.1093/cid/civ307

10 Nimmerjahn, F. & Ravetch, J. V. Fcγ receptors as regulators of immune responses. *Nature Reviews Immunology* **8**, 34–47 (2008). https://doi.org/10.1038/nri2206

11 Delidakis, G., Kim, J. E., George, K. & Georgiou, G. Improving Antibody Therapeutics by Manipulating the Fc Domain: Immunological and Structural Considerations. *Annual Review of Biomedical Engineering* **24**, 249–274 (2022). https://doi.org/10.1146/annurev-bioeng-082721-024500

12 Pyzik, M., Kozicky, L. K., Gandhi, A. K. & Blumberg, R. S. The therapeutic age of the neonatal Fc receptor. *Nature Reviews Immunology* **23**, 415–432 (2023). https://doi.org/10.1038/s41577-022-00821-1

13 Chen, X., Schneewind, O. & Missiakas, D. Engineered human antibodies for the opsonization and killing ofStaphylococcus aureus. *Proceedings of the National Academy of Sciences* **119** (2022). https://doi.org/10.1073/pnas.2114478119

14 Dall'Acqua, W. F., Kiener, P. A. & Wu, H. Properties of Human IgG1s Engineered for Enhanced Binding to the Neonatal Fc Receptor (FcRn). *Journal of Biological Chemistry* **281**, 23514–23524 (2006). https://doi.org/10.1074/jbc.M604292200

15 Domachowske, J. B. *et al.* Safety, Tolerability and Pharmacokinetics of MEDI8897, an Extended Half-life Single-dose Respiratory Syncytial Virus Prefusion F-targeting Monoclonal Antibody Administered as a Single Dose to Healthy Preterm Infants. *Pediatric Infectious Disease Journal* **37**, 886–892 (2018). https://doi.org/10.1097/inf.0000000000001916

16 Mu, X. *et al.* The Effect of Colistin Resistance-Associated Mutations on the Fitness of Acinetobacter baumannii. *Frontiers in Microbiology* **7** (2016). https://doi.org/10.3389/fmicb.2016.01715

17 Novović, K. & Jovčić, B. Colistin Resistance in Acinetobacter baumannii: Molecular Mechanisms and Epidemiology. *Antibiotics* **12** (2023). https://doi.org/10.3390/antibiotics12030516

18 Boxx, Gayle M. & Cheng, G. The Roles of Type I Interferon in Bacterial Infection. *Cell Host & Microbe* **19**, 760–769 (2016). https://doi.org/10.1016/j.chom.2016.05.016

19 Liu, X. *et al.* Activation of the JAK/STAT-1 Signaling Pathway by IFN-γ Can Down-Regulate Functional Expression of the MHC Class I-Related Neonatal Fc Receptor for IgG. *The Journal of Immunology* **181**, 449–463 (2008). https://doi.org/10.4049/jimmunol.181.1.449

20 Szijártó, V. *et al.* Bactericidal Monoclonal Antibodies Specific to the Lipopolysaccharide O Antigen from Multidrug-Resistant Escherichia coli Clone ST131-O25b:H4 Elicit Protection in Mice. *Antimicrobial Agents and Chemotherapy* **59**, 3109–3116 (2015). https://doi.org/10.1128/aac.04494-14

21 Shankar-Hari, M. *et al.* Endogenous IgG hypogammaglobulinaemia in critically ill adults with sepsis: systematic review and meta-analysis. *Intensive Care Medicine* **41**, 1393–1401 (2015). https://doi.org/10.1007/s00134-015-3845-7

22 Roopenian, D. C. & Akilesh, S. FcRn: the neonatal Fc receptor comes of age. *Nature Reviews Immunology* **7**, 715–725 (2007). https://doi.org/10.1038/nri2155

23 Lee, S.-h. S., Phyllis. Gordon, Siamon. . Quantitative analysis of total macrophage content in adult mouse tissues. Immunochemical studies with monoclonal antibody F4/80. *The Journal of experimental medicine* **161**, 475–489 (1985). https://doi.org/10.1084/jem.161.3.475

24 Challa, D. K. *et al.* Neonatal Fc receptor expression in macrophages is indispensable for IgG homeostasis. *mAbs* **11**, 848–860 (2019). https://doi.org/10.1080/19420862.2019.1602459

25 Zhao, X. *et al.* Human Neonatal Fc Receptor Is the Cellular Uncoating Receptor for Enterovirus B. *Cell* **177**, 1553–1565.e1516 (2019). https://doi.org/10.1016/j.cell.2019.04.035

26 Li, F. *et al.* Establishment of disseminated neonatal echovirus 11 infection model in hFcRn transgenic mice. *Virology Journal* **22** (2025). https://doi.org/10.1186/s12985-025-02979-1

27 Haga, K. *et al.* Neonatal Fc receptor is a functional receptor for classical human astrovirus. *Genes to Cells* **29**, 983–1001 (2024). https://doi.org/10.1111/gtc.13160

28 Liu, X. *et al.* Human cytomegalovirus evades antibody-mediated immunity through endoplasmic reticulum-associated degradation of the FcRn receptor. *Nature Communications* **10** (2019). https://doi.org/10.1038/s41467-019-10865-y

29 Qian, S. *et al.* Downregulation of FcRn promotes ferroptosis in herpes simplex virus-1-induced lung injury. *Cellular and Molecular Life Sciences* **82** (2025). https://doi.org/10.1007/s00018-024-05555-y

30 Cejas, R. B., Ferguson, D. C., Quiñones-Lombraña, A., Bard, J. E. & Blanco, J. G. Contribution of DNA methylation to the expression of FCGRT in human liver and myocardium. *Scientific Reports* **9** (2019). https://doi.org/10.1038/s41598-019-45203-1

31 Cecconi, M., Evans, L., Levy, M. & Rhodes, A. Sepsis and septic shock. *The Lancet* **392**, 75–87 (2018). https://doi.org/10.1016/s0140-6736(18)30696-2

32 Angus, D. C. *et al.* E5 murine monoclonal antiendotoxin antibody in gram-negative sepsis: a randomized controlled trial. *Jama* **283**, 1723–1730 (2000).

33 Reinhart, K. *et al.* CD14 receptor occupancy in severe sepsis: Results of a phase I clinical trial with a recombinant chimeric CD14 monoclonal antibody (IC14)*. *Critical Care Medicine* **32**, 1100–1108 (2004). https://doi.org/10.1097/01.Ccm.0000124870.42312.C4

34 Harrison, M. L. *et al.* Tumor Necrosis Factor α As a New Target for Renal Cell Carcinoma: Two Sequential Phase II Trials of Infliximab at Standard and High Dose. *Journal of Clinical Oncology* **25**, 4542–4549 (2007). https://doi.org/10.1200/jco.2007.11.2136

35 McCarthy, M. W., Chong, C., Riedemann, N. C. & Guo, R. A Targeted Blockade of Terminal C5a Is Critical to Management of Sepsis and Acute Respiratory Distress Syndrome: The Mechanism of Action of Vilobelimab. *International Journal of Molecular Sciences* **26** (2025). https://doi.org/10.3390/ijms26199628

36 Briassouli, E., Syrimi, N. & Ilia, S. Hyperferritinemia and Macrophage Activation Syndrome in Septic Shock: Recent Advances with a Pediatric Focus (2020–2025). *Children* **12** (2025). https://doi.org/10.3390/children12091193

37 Vlaar, A. P. J. *et al.* Anti-C5a antibody IFX-1 (vilobelimab) treatment versus best supportive care for patients with severe COVID-19 (PANAMO): an exploratory, open-label, phase 2 randomised controlled trial. *The Lancet Rheumatology* **2**, e764–e773 (2020). https://doi.org/10.1016/s2665-9913(20)30341-6

38 Hotchkiss, R. S., Monneret, G. & Payen, D. Immunosuppression in sepsis: a novel understanding of the disorder and a new therapeutic approach. *The Lancet Infectious Diseases* **13**, 260–268 (2013). https://doi.org/10.1016/s1473-3099(13)70001-x

39 Giamarellos-Bourboulis, E. J. *et al.* The pathophysiology of sepsis and precision-medicine-based immunotherapy. *Nature Immunology* **25**, 19–28 (2024). https://doi.org/10.1038/s41590-023-01660-5

40 Gong, N. *et al.* Mannich reaction-based combinatorial libraries identify antioxidant ionizable lipids for mRNA delivery with reduced immunogenicity. *Nature Biomedical Engineering* (2025). https://doi.org/10.1038/s41551-025-01422-8

41 Guan, X. *et al.* Engineered M2 macrophage-derived exosomes: mechanisms and therapeutic potential in inflammation regulation and regenerative medicine. *Acta Biomaterialia* **203**, 38–58 (2025). https://doi.org/10.1016/j.actbio.2025.07.039

42 Zhang, H., Liu, D., Yang, K., Liang, Z. & Li, M. Ionizable guanidine-based lipid nanoparticle for targeted mRNA delivery and cancer immunotherapy. *Science Advances* **11**, eadx5970 (2025).

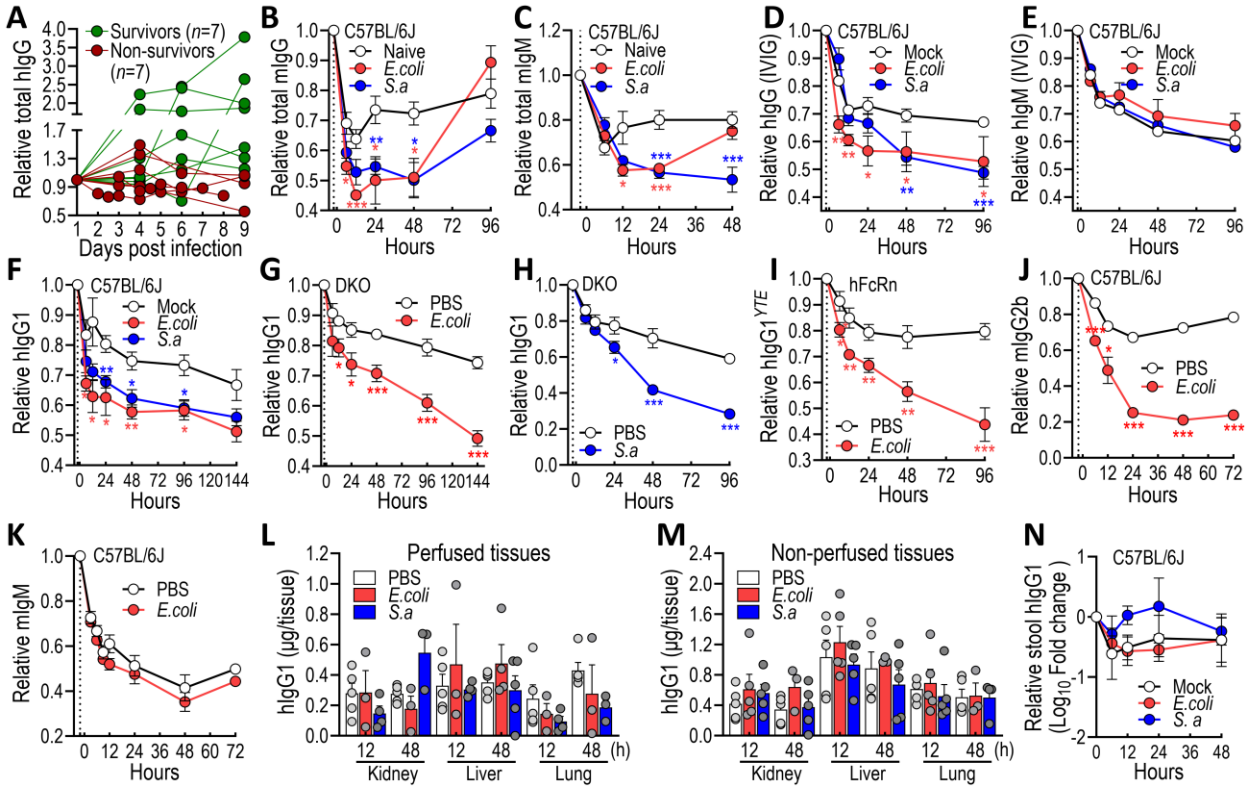

Fig. 1. Bacterial sepsis drives the loss of both endogenous and exogenous IgG. (**A**) Relative abundance of serum IgG in bacterial sepsis patients (survivors vs. non-survivors, n = 7 per group) over time. (**B** and **C**) Serum kinetics of total mIgG (B, *n* = 5) and mIgM (C, *n* = 10) in C57BL/6J mice with sepsis induced by pathogenic *E. coli* (1×10^8 CFU/mouse) or *S. aureus* Δ*spa*Δ*sbi*Δ*ssl10* (1×10^7 CFU/mouse), respectively. These inocula were used unless otherwise specified. (**D** and **E**) Serum hIgG (D) and hIgM (E) kinetics in IVIG (500 μg/mouse)-treated C57BL/6J mice (*n* = 5) during sepsis induced by pathogenic *E. coli* or *S. aureus* Δ*spa*Δ*sbi*Δ*ssl10*. (**F**) Serum hIgG1 kinetics in C57BL/6J mice (*n* = 5) following its administration and subsequent septic challenge with pathogenic *E. coli* or *S. aureus* Δ*spa*Δ*sbi*Δ*ssl10*. A dose of 100 μg mAb per mouse was used throughout (unless specified). (**G** and **H**) Serum hIgG1 kinetics in IgD & IgM double knockout C57BL/6J mice (*n* = 10) following its administration and subsequent septic challenge with pathogenic *E. coli* (G) or *S. aureus* Δ*spa*Δ*sbi*Δ*ssl10* (H). (**I**) Serum hIgG1^{YTE} kinetics in humanized FcRn C57BL/6N mice (*n* = 10) following its administration and subsequent septic

challenge with pathogenic *E. coli*. (**J** and **K**) Serum kinetics of mIgG2b (J) or mIgM (K) mAb in C57BL/6J mice (n = 4 and 8) following its administration and subsequent septic challenge with pathogenic *E. coli*. (**L** and **M**) Concentration of exogenous hIgG1 in perfused (L) and non-perfused (M) murine tissues (n = 3 to 5) at 12 and 48 hours after septic challenge. (**N**) Relative levels of exogenous hIgG1 in murine feces (n = 5) at different times after septic challenge. Data are presented as mean ± SEM. Significant differences (*$p < 0.05$, **$p < 0.01$, and ***$p < 0.001$) were identified in B-D and F-J by two-tailed Student's t test.

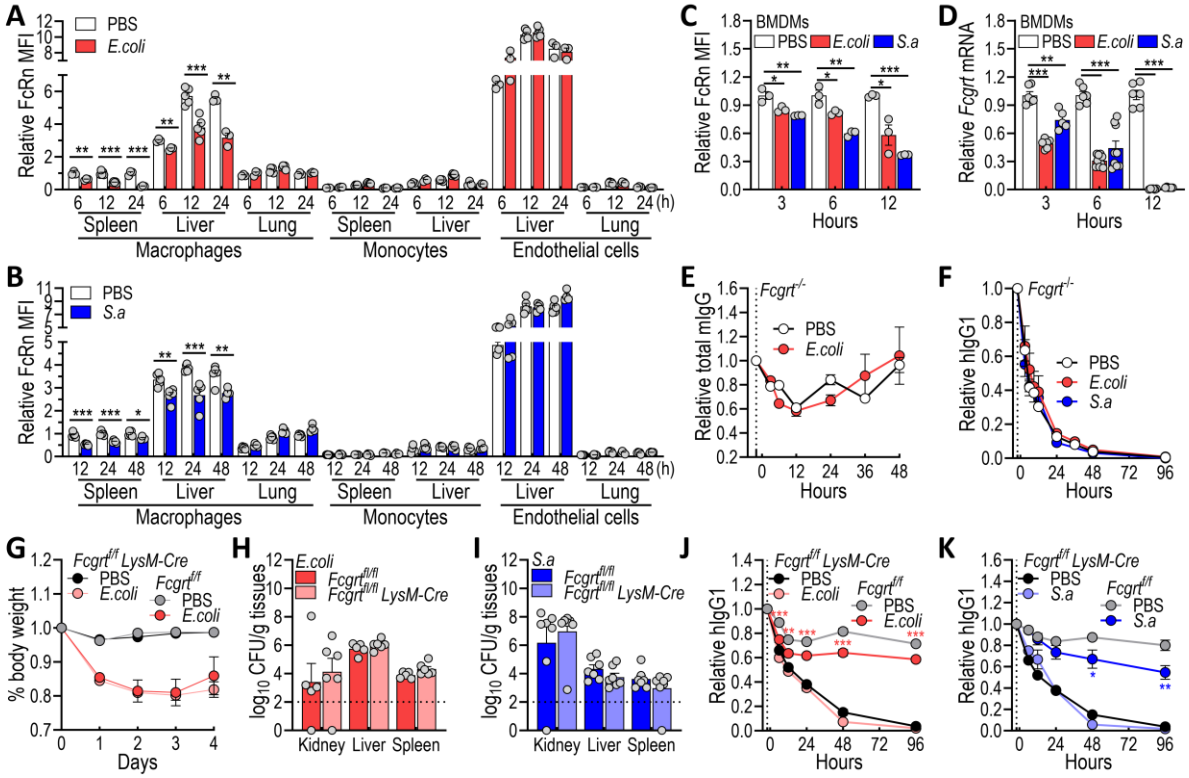

Fig. 2. Loss of macrophage FcRn mediates circulating IgG loss in septic mice. (**A** and **B**) Flow cytometric analysis of relative FcRn expression in macrophages, monocytes, and endothelial cells from murine tissues (n = 3 to 5) at indicated times after septic challenge with *E. coli* (A) or *S. aureus* Δ*spa*Δ*sbi*Δ*ssl10* (B). (**C** and **D**) Flow cytometric (C, n = 3) and qPCR (D, n = 6 to 9) analysis of relative FcRn expression in bone marrow-derived macrophages (BMDMs) after *E. coli* (MOI 1) or *S. aureus* Δ*spa*Δ*sbi*Δ*ssl10* (MOI 5) infection. (**E**) Serum total mIgG kinetics in *Fcgrt*$^{-/-}$ C57BL/6J mice (n = 6) with *E. coli*-induced sepsis. (**F**) Serum hIgG1 kinetics in *Fcgrt*$^{-/-}$ C57BL/6J mice (n = 5 to 8) following its administration and subsequent septic challenge with *E. coli* or *S. aureus* Δ*spa*Δ*sbi*Δ*ssl10*. (**G**) Relative body weight in *Fcgrt*$^{f/f}$ and *Fcgrt*$^{f/f}$ *LysM-Cre* C57BL/6J mice (n = 6) with pathogenic *E. coli*-induced sepsis. (**H** and **I**) Bacterial loads in tissues from *Fcgrt*$^{f/f}$ and *Fcgrt*$^{f/f}$ *LysM-Cre* C57BL/6J mice (n = 5 to 7) at 96 hours after septic challenge with *E. coli* (H) or *S. aureus* Δ*spa*Δ*sbi*Δ*ssl10* (I). (**J** and **K**) Serum hIgG1 kinetics in *Fcgrt*$^{f/f}$ and *Fcgrt*$^{f/f}$ *LysM-Cre* C57BL/6J mice (n = 6 to 12) following its administration and subsequent septic

challenge with *E. coli* (J) or *S. aureus* Δ*spa*Δ*sbi*Δ*ssl10* (K). Data are presented as mean ± SEM. Significant differences (*p < 0.05, **p < 0.01, and ***p < 0.001) were identified in A, B, J, and K by two-tailed Student's *t* test and in C and D by one-way ANOVA analysis.

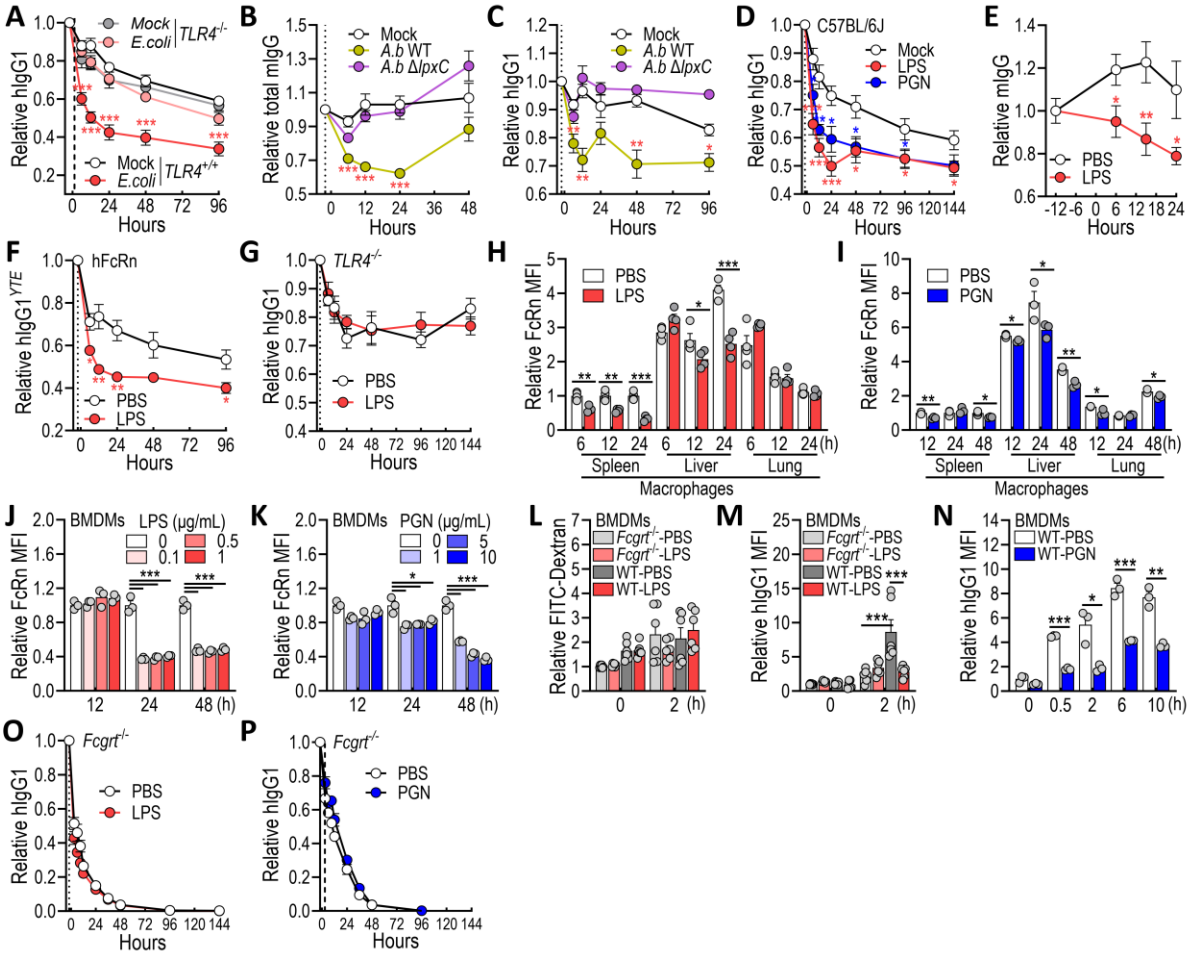

Fig. 3. Bacterial LPS and PGN induce FcRn downregulation and IgG loss in mice. (**A**) Serum hIgG1 kinetics in *TLR4*$^{+/+}$ and *TLR4*$^{-/-}$ C57BL/6J mice (n = 5) following its administration and subsequent septic challenge with *E. coli*. (**B**) Serum total mIgG kinetics in C57BL/6J mice (n = 5) with *Acinetobacter baumannii* wild-type- or Δ*lpxC*-induced sepsis. (**C**) Serum hIgG1 kinetics in C57BL/6J mice (n = 5) following its administration and subsequent septic challenge with *Acinetobacter baumannii* wild-type (2×10^8 CFU/mouse) or Δ*lpxC* (6×10^8 CFU/mouse). (**D**) Serum hIgG1 kinetics in C57BL/6J mice (n = 11 to 15) following its administration and subsequent challenge with LPS (5 mg/kg) or PGN (10 mg/kg). (**E**) Serum total mIgG kinetics in C57BL/6J mice (n = 17) with LPS (5 mg/kg) challenge. (**F**) Serum hIgG1^{YTE} kinetics in humanized FcRn C57BL/6N mice (n = 4) following its administration and subsequent LPS (5 mg/kg) challenge. (**G**)

Serum hIgG1 kinetics in *TLR4*$^{-/-}$ mice (n = 8) following its administration and subsequent LPS (5 mg/kg) challenge. (**H** and **I**) Flow cytometric analysis of relative FcRn expression in macrophages isolated from murine tissues at indicated times after LPS (H, 5 mg/kg, n = 4) or PGN (I, 10 mg/kg, n = 3) challenge. (**J** and **K**) Flow cytometric analysis of relative FcRn expression in BMDMs (n = 3 to 5) after challenge with LPS (J) or PGN (K) at indicated times and doses. (**L**) Phagocytic analysis of FITC-dextran uptake by LPS-treated BMDMs (n = 6) from WT and *Fcgrt*$^{-/-}$ mice. (**M**) Determination of hIgG1 (Alexa Fluor 647-labeled) in LPS-treated BMDMs (n = 3) from WT and *Fcgrt*$^{-/-}$ mice by flow cytometry. (**N**) Determination of hIgG1 (Alexa Fluor 647-labeled) in PGN-treated BMDMs (n = 3) from WT mice by flow cytometry. (**O** and **P**) Serum hIgG1 kinetics in *Fcgrt*$^{-/-}$ C57BL/6J mice (n = 11 to 15) following its administration and subsequent challenge with LPS (M, 5 mg/kg) or PGN (N**,** 10 mg/kg). Data are presented as mean ± SEM. Significant differences (*p < 0.05, **p < 0.01, and ***p < 0.001) were identified in A to F, H, I, and N by two-tailed Student's t test and in J, K, and M by one-way ANOVA analysis.

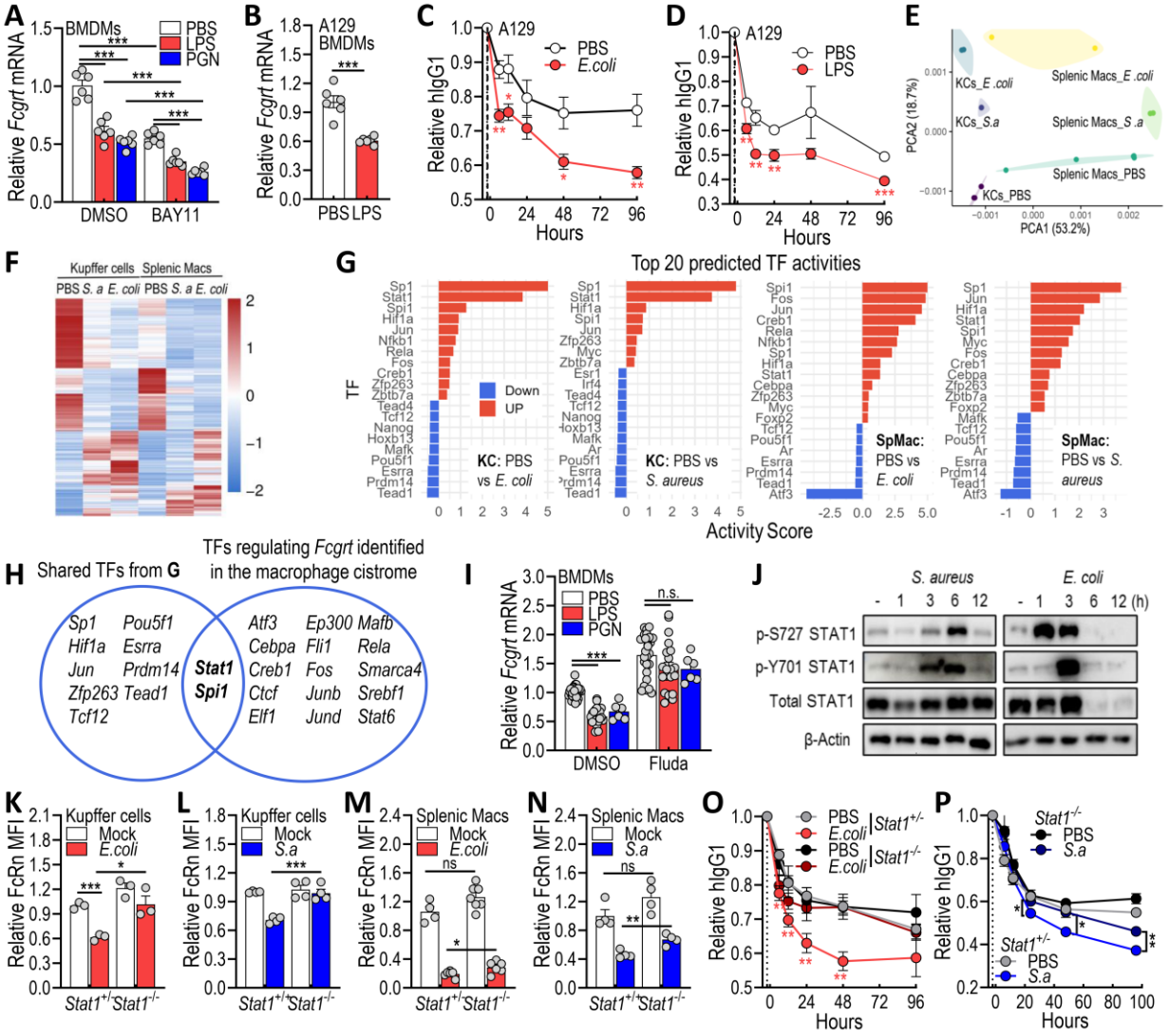

Fig. 4. STAT1 activation mediates macrophage FcRn reduction and IgG loss in septic mice. (**A**) Effect of NF-κB inhibitor BAY11-7082 (BAY11, 10 μM) on *Fcgrt* expression in BMDMs (n = 6) treated with LPS (1 μg/ml) or PGN (10 μg/ml) for 12h. (**B**) qPCR analysis of *Fcgrt* expression in A129 mouse-derived BMDMs (n = 6) treated with LPS (1 μg/ml) for 12h. (**C** and **D**) Serum hIgG1 kinetics in A129 mice (n = 5) following its administration and subsequent challenge with *E. coli* (C) or LPS (D**,** 5 mg/kg). **(E)** Principal component analysis (PCA) of transcriptomic data from kupffer cells (KCs) and splenic macrophages (Macs) of septic mice induced by pathogenic *E. coli* or *S. aureus* Δ*spa*Δ*sbi*Δ*ssl10*. **(F)** Heat-map of shared sepsis-induced differentially expressed genes (DEGs) in kupffer cells and splenic macrophages. **(G)** Transcription factor (TF)

activity inferred from shared DEGs. KC, Kupffer cell; SpMac: splenic macrophages. **(H)** Venn diagram showing the overlap between *Fcgrt*-regulating TFs identified from the macrophage cistrome and functionally inferred TFs from the shared DEGs. (**I**) qPCR analysis of *Fcgrt* expression in BMDMs (n = 5 to 27) treated with STAT1 inhibitor Fludarabine (50 μM) and stimulated with LPS (1 μg/ml) or PGN (10 μg/ml) for 12 h. (**J**) Western blotting analysis of STAT1 phosphorylation in BMDMs treated with *E. coli* (MOI 1) or *S. aureus* Δ*spa*Δ*sbi*Δ*ssl10* (MOI 5). β-actin was used as the loading control. (**K** to **N**) Flow cytometric analysis of relative FcRn expression in liver (K, L) and splenic (M, N) macrophages isolated from *Stat1*$^{-/-}$ mice and their controls (n = 3 to 5) at 24 hours after septic challenge with *E. coli* (K, M) or *S. aureus* Δ*spa*Δ*sbi*Δ*ssl10* (L, N). (**O** and **P**) Serum hIgG1 kinetics in *Stat1*$^{+/-}$ and *Stat1*$^{-/-}$mice (n = 10) following its administration and subsequent septic challenge with pathogenic *E. coli* (O) or *S. aureus* Δ*spa*Δ*sbi*Δ*ssl10* (P). Data are presented as mean ± SEM. Significant differences (*p < 0.05, **p < 0.01, and ***p < 0.001) were identified in A, I, K, L, M, and N by two-way ANOVA analysis, in B, C, D, O, and P by two-tailed Student's *t* test, and in I by one-way ANOVA analysis.

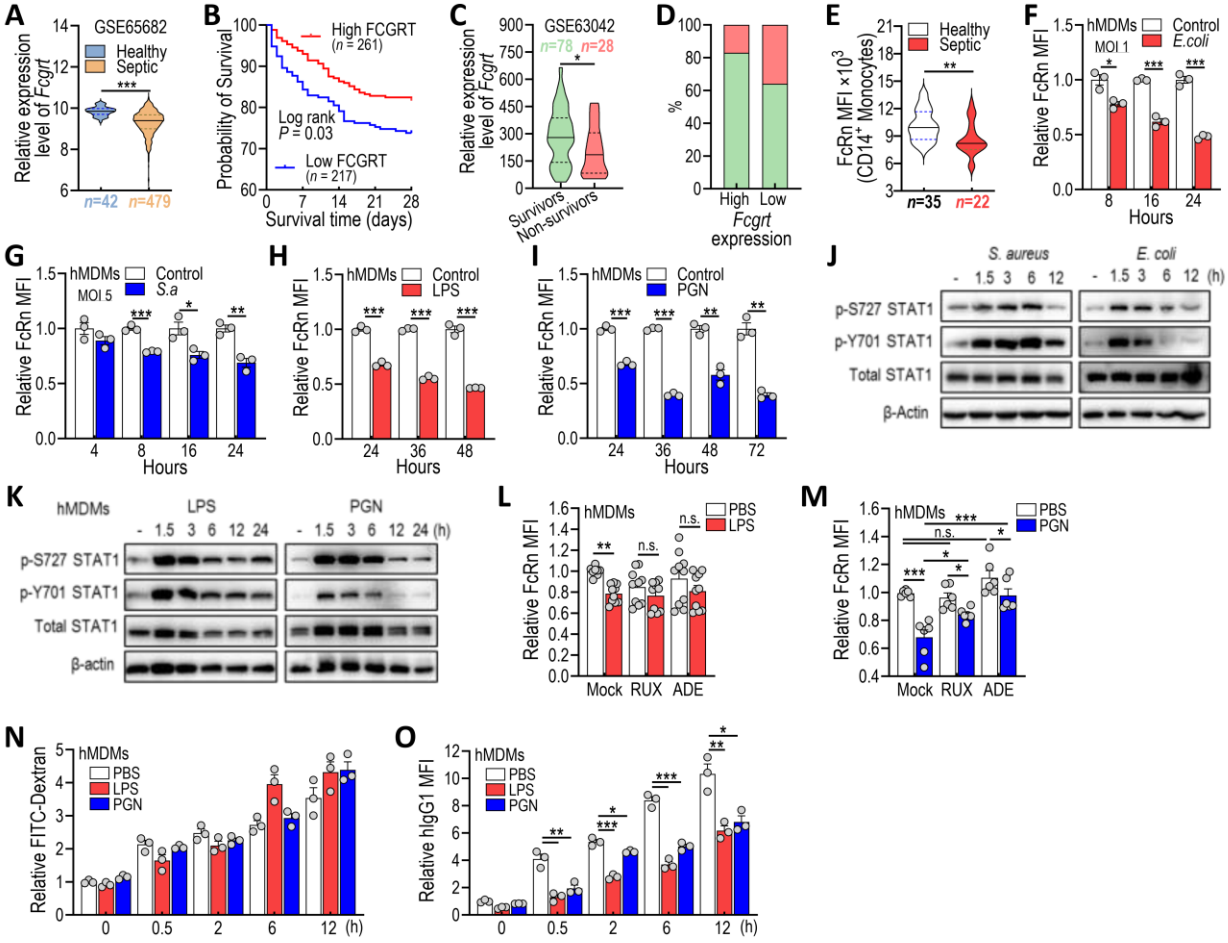

Fig. 5. FcRn reduction and resultant IgG loss driven by STAT1 signaling are conserved in humans. (**A**) Analysis of *Fcgrt* expression in a public dataset (GSE65682) of whole-blood leukocytes from healthy donors and septic patients. (**B**) Assessment of survival probability of septic patients with low vs. high *Fcgrt* expression levels by analyzing the GSE65682 dataset. (**C**) Analysis of *Fcgrt* expression in a public dataset (GSE63042) of whole blood from bacterial sepsis survivors (n = 78) and non-survivors (n = 28). (**D**) Proportion assessment of bacterial sepsis survivors (n = 78) and non-survivors (n = 28) with low or high *Fcgrt* expression by analyzing the GSE63042 dataset. (**E**) Flow cytometric analysis of FcRn expression in $CD14^+$ monocytes isolated from healthy donors (n = 35) and patients with bacterial sepsis (n = 22). (**F** to **I**) Flow cytometric analysis of FcRn expression in $CD14^+$ monocyte-derived macrophages (hMDMs, n = 3) at

indicated times after challenge with *E. coli* (F**,** MOI 1), *S. aureus* Δ*spa*Δ*sbi*Δ*ssl10* (G, MOI 5), LPS (H**,** 1 μg/ml) or PGN (I, 10 μg/ml). (**J** and **K**) Western blotting analysis of STAT1 phosphorylation in hMDMs treated with *E. coli* (J**,** MOI 1), *S. aureus* Δ*spa*Δ*sbi*Δ*ssl10* (J**,** MOI 5), LPS (K**,** 1 μg/ml), or PGN (K**,** 10 μg/ml). β-actin was used as the loading control. (**L** and **M**) Flow cytometric analysis of relative FcRn expression in hMDMs pretreated with STAT1 phosphorylation inhibitors RUX (Ruxolitinib, targeting Tyr701) or ADE (Adezmapimod, targeting Ser727) and stimulated with LPS (L, n = 10) or PGN (M, n = 6) for 24 h. (**N**) Phagocytic analysis of FITC-dextran uptake by LPS- or PGN-treated hMDMs (n = 3). (**O**) Determination of hIgG1 (Alexa Fluor 647-labeled) in LPS- or PGN-treated hMDMs (n = 3). Data are presented as mean ± SEM. Significant differences (*p < 0.05, **p < 0.01, and ***p < 0.001) were identified in A, C, and E by two-tailed Student's *t* test, in B by the Kaplan-Meier survival analysis with the log-rank test, and in F, G, H, I, L, M and O by two-way ANOVA analysis.

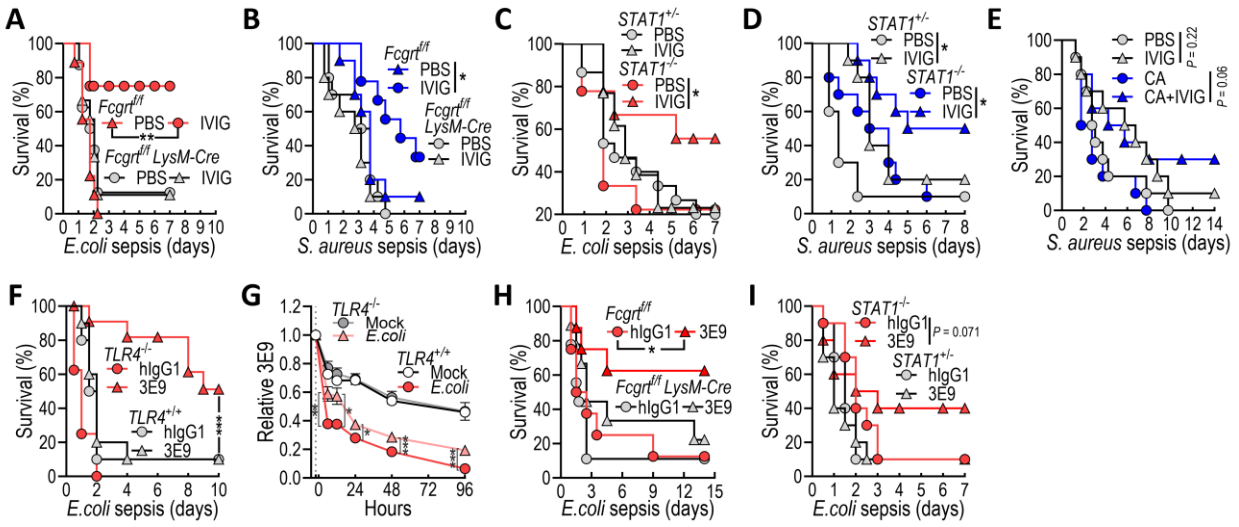

Fig. 6. Antibody efficacy in bacterial sepsis is rescued by inhibiting STAT1-driven FcRn suppression. (**A** and **B**) Survival of *Fcgrt*$^{f/f}$ and *Fcgrt*$^{f/f}$ *LysM-Cre* C57BL/6J mice (n = 8 to 10) treated with PBS or IVIG following sepsis induced by *E. coli* (A, 3 × 10^8 CFU/mouse) or *S. aureus* Δ*spa*Δ*sbi*Δ*ssl10* (B, 5 × 10^7 CFU/mouse). IVIG was administered at 600 μg for *E. coli* and 900 μg for *S. aureus* challenges. These bacterial inocula and IVIG doses were used consistently unless stated otherwise. (**C** and **D**) Survival of *STAT1*$^{+/-}$ and *STAT1*$^{-/-}$ C57BL/6J mice (n = 9 to 15) treated with PBS or IVIG following sepsis induced by *E. coli* **(C)** or *S. aureus* Δ*spa*Δ*sbi*Δ*ssl10* **(D)**. (**E**) Survival of ICR (n = 10) mice pretreated with PBS or IVIG followed by carnosic acid (CA) prior to sepsis induction with *S. aureus* Δ*spa*Δ*sbi*Δ*ssl10*. (**F**) Survival of *TLR4*$^{+/+}$ and *TLR4*$^{-/-}$ C57BL/6J mice (n = 10) treated with hIgG1 or 3E9 following sepsis induced by *E. coli*. hIgG1 and 3E9 were administrated at a dose of 200 μg per mouse. (**G**) Serum 3E9 kinetics in *TLR4*$^{+/+}$ and *TLR4*$^{-/-}$ C57BL/6J mice (n = 5) following its administration and subsequent septic challenge with *E. coli*. **(H)** Survival of *Fcgrt*$^{f/f}$ and *Fcgrt*$^{f/f}$ *LysM-Cre* C57BL/6J mice (n = 8 to 9) treated with hIgG1 or 3E9 following sepsis induced by *E. coli*. hIgG1 and 3E9 were administrated at a dose of 500 μg per mouse. (**I**) Survival of *STAT1*$^{+/-}$ and *STAT1*$^{-/-}$ C57BL/6J mice (n = 8 to 10) treated with hIgG1 or 3E9 following sepsis induced by *E. coli*. hIgG1 and 3E9 were administrated at a dose of 200 μg

per mouse. Data are presented as mean ± SEM. Significant differences (*p < 0.05, **p < 0.01, and ***p < 0.001) were identified in A-F, H, and I by the Kaplan-Meier survival analysis with the log-rank test and in G by two-tailed Student's *t* test.

Materials and Methods

Ethnic statement

The Shenzhen Bay Laboratory Medical Ethical Committee reviewed, approved, and supervised the protocol (No. YL 2024-017) used for all experiments utilizing blood from human volunteers and informed consent forms were obtained from all participants. Animal research was performed in accordance with institutional guidelines following experimental protocol review, approval, and supervision by the Institutional Animal Care and Use Committee at the Shenzhen Bay Laboratory (Approval No. AECXH202201). Experiments with pathogenic *Escherichia coli*, *Staphylococcus aureus*, and *Acinetobacter baumannii* were performed in biosafety level 2 (BSL2)/animal BSL2 (ABSL2) containment upon review by Shenzhen Bay Laboratory Institutional Biosafety Committee.

Mice

All immunization and infection experiments were conducted in sex-matched mice, including the C57BL/6J, ICR (procured from GemPharmatech), and various genetically modified strains. With the exception of the humanized FcRn (hFcRn, C57BL/6N) and A129 mice, all genetically modified mice were maintained on a C57BL/6J background. Mice with C57BL/6J or C57BL/6N background were housed under specific pathogen-free conditions with *ad libitum* access to water and standard chow. Specifically, FcRn knockout (KO) (*Fcgrt*$^{-/-}$; #NM-KO-00133) was kindly provided by Dr. Jingren Zhang at the Tsinghua University [43] and bred in our animal facility. STAT1 KO (*Stat1*$^{-/-}$; #NM-KO-200611) and *Fcgrt* floxed (#NM-CKO-200094) mice were obtained from the Model Organisms Center. The *LsyM-Cre* (#004781) strain was sourced from Jackson Laboratory. The IgM & IgD double KO (DKO; #C001342) and hFcRn (#C001701) mice

were acquired from Cyagen. The TLR4 KO (*TLR4*$^{-/-}$; #N000192) mice were purchased from GemPharmatech. The A129 mice were a generous gift from Dr. Yang Liu within our institution.

Bacteria

The *S. aureus* Δ*spa*Δ*sbi*Δ*ssl10* mutant used in this study is maintained in our laboratory and was originally provided by Dr. Dominique Missiakas (The University of Chicago). The pathogenic *E. coli* BSI099 strain was a kind gift from Dr. Guobao Tian (Sun Yat-sen University), and the isogenic *lpxC* mutant was previously constructed in the *A. baumannii* ATCC 17978 background [16]. For routine culture, *S. aureus* was grown in tryptic soy broth (TSB) or on TSB agar, while both *E. coli* and *A. baumannii* were cultivated in Luria broth (LB) or on LB agar; all strains were incubated at 37°C.

Antibodies

Commercial intravenous immunoglobulin (IVIG), composed of >95% human IgG (hIgG) with a specified 1-3% human IgM (hIgM) content, was purchased from Chengdu Rongsheng Pharmaceuticals (#S20237008). Monoclonal mouse IgG2b and IgM antibodies specific for Keyhole Limpet Hemocyanin (KLH) were purchased from Absea Biotechnology (Cat. No. K06036M09G11C and K06036M01E09C, respectively). The hIgG1 used in this study is a recombinant human monoclonal antibody (mAb) targeting SpA_{KKAA}, a variant of the *S. aureus* protein A (SpA) encoded by the *spa* gene [44,45]. The hIgG1^{YTE} was engineered to contain M252Y/S254T/T256E (YTE) mutations in the Fc portion of hIgG1. Primers 5‘-TACATCACACGGGAGCCTGAGGTCACATGCGTGGT-3’ and 5’-CTCCCGTGTGATGTAGAGGGTGTCCTTGGGTTTTG-3’ were used to generate the YTE variant in the previously constructed pVITRO1 plasmid encoding hIgG1 (*45*). The variable heavy

and light chain genes of 3E9 and anti-FcRn antibody (formerly known as SYNT001) were synthesized from published sequences [20,46] by GENERAL BIOL (Chuzhou, China) and swapped into the pVITRO1-102.1F10-IgG1/λ plasmid (Addgene, #50366). Plasmids were transfected into HEK-293F cells using polyethylenimine, followed by selection with hygromycin B (400 μg/mL) and expansion of stable transfectants. Antibodies were affinity purified from supernatants of expanded cultures on protein G resin (GenScript) and dialyzed against PBS as described (*13*). The anti-FcRn antibody was labeled with Elab Fluor® 647 (EF647) NHS ester (succinimidyl ester; Elabscience, #E-LK-E006C) according to the manufacturer's instructions. Additional antibodies used for flow cytometry or Western blot are described in the following sections.

Mouse sepsis model

A monomicrobial murine sepsis model was generated using *S. aureus*, *E. coli*, or *A. baumannii*. Briefly, *S. aureus* cultures were grown to OD_{600} 0.45 and *E. coli* and *A. baumannii* to OD_{600} 1.0, pelleted, washed once in PBS, and resuspended to the desired CFU/ml. Mice received 100 μl of inoculum via the retro-orbital plexus (*S. aureus*, *E. coli*) or intraperitoneally (*A. baumannii*) under anesthesia. Animals were monitored daily for clinical signs and weight loss. At predefined time points, serum and liver, kidney, and spleen samples were collected. Serum Ig levels were quantified, and tissues were weighed, homogenized, diluted, and plated to determine bacterial burdens (CFU/g). Survival was recorded to assess antibody efficacy.

Antibody concentration assay

Antibody concentrations were determined by enzyme-linked immunosorbent assay (ELISA) as follows. To quantify endogenous hIgG in human serum or exogenous hIgG in mouse serum, microtiter plates were coated overnight with 200 ng/well goat anti-hIgG-Fcγ (Jackson

ImmunoResearch, #109-005-008) and blocked. The wells were then incubated with a 1:2,500,000 dilution of human serum or a 1: 50,000 dilution of serum from mice treated with 500 μg IVIG, followed by an HRP-conjugated goat anti-hIgG-F(ab')^2 antibody (Jackson ImmunoResearch, #109-035-006). For measuring endogenous mouse IgG and IgM, microtiter plates were coated overnight with 30,000× (for mIgG) or 5,000× (for mIgM) dilution of serum sample. After blocking, the plates were incubated with HRP-conjugated goat anti-mIgG (Jackson ImmunoResearch, #115-035-003) or -mIgM (Invitrogen, #62-6820). To measure the pharmacokinetics of injected antibodies (hIgG1, hIgG1^{YTE}, mIgG2b, or mIgM), mice were injected into the peritoneal cavity with 100 μg test mAb. Serum was collected at indicated time points post-injection, and antibody concentrations were detected using antigen-coated plates (SpA$_{KKAA}$ or KLH) and matched HRP-conjugated secondary antibodies (Promega, #W403B; Jackson ImmunoResearch, #115-035-003; Invitrogen, #62-6820). For tissue antibody quantification, samples were processed under perfused and non-perfused conditions. Intracardiac perfusion was performed in anesthetized mice via the left ventricle at a constant rate of 4 ml/min using PBS until the tissues appeared visibly pale and the lungs turned white. Both perfused and non-perfused tissues, as well as mouse fecal samples, were weighed and homogenized in PBS containing 0.1% Triton X-100 using a Tissuelyser II (Qiagen). The homogenates were centrifuged, and the supernatants were appropriately diluted and applied to SpA$_{KKAA}$-coated microtiter plates. All antibody concentrations were calculated from standard curves ranging from 0.1 ng/ml to 10 μg/ml. Human IgM levels were determined using a commercial ELISA kit (Mabtech, #3880-1AD-6). All plates were developed using TMB Chromogen Solution (Sangon Biotech). Recombinant SpA$_{KKAA}$ was purified from *E. coli* as described (*44*), and KLH was purchased from ThermoFisher (#77600).

Flow cytometric analysis of FcRn, FcγRs, and CRs expression

Single-cell suspensions were prepared from mouse spleen, liver, lung, and blood. Spleens were harvested and gently mashed through a 70-μm cell strainer in RPMI-1640 medium. The resulting splenocytes were treated with red blood cell (RBC) lysis buffer (Biosharp, #B541001-0100) for 2 minutes on ice. After lysis, cells were washed and resuspended in PBS containing 2 mM EDTA for subsequent use. Liver non-parenchymal cells (NPCs) were isolated using a modified collagenase-DNase digestion protocol [47]. Briefly, mice were euthanized, and livers were perfused *via* the portal vein with PBS, excised, and mechanically dissociated in digestion buffer (RPMI 1640 with 0.5 mg/ml collagenase IV, 20 μg/ml DNase I, and 0.5 mM $CaCl_2$) using a tissue dissociator (RWD Life Science). The homogenate was filtered through a 70-μm strainer and washed. The cell pellet was treated with RBC lysis buffer on ice for 3 minutes, and the reaction was quenched with RPMI 1640 medium. The suspension was centrifuged at 60 ×g for 2 minutes to pellet hepatocytes, and the supernatant containing enriched NPCs was collected. Lung tissues were excised and subjected to mechanical and enzymatic dissociation in digestion buffer (RPMI 1640 with 0.5 mg/ml collagenase IV, 50 μg/ml DNase I, and 0.5 mM $CaCl_2$) using a tissue dissociator (RWD Life Science). The homogenate was filtered through a 70-μm strainer, washed, and subjected to RBC lysis. Finally, the cells were resuspended in PBS with 2 mM EDTA. Blood was collected via the retro-orbital plexus. After RBC lysis, immune cells were washed and resuspended in PBS with 2 mM EDTA. Prior to staining, single-cell suspensions were labeled with a fixable viability dye (ThermoFisher, #eF506) and blocked with an anti-CD16/32 antibody (Biolegend, #156604). Surface staining was performed sequentially, starting with anti-Ly-6G/6C antibodies, followed by a cocktail of other surface markers. For intracellular FcRn staining, cells were fixed, permeabilized (ThermoFisher, #88-8824-00), and stained with an EF647-conjugated anti-FcRn antibody (made in-house). For FcγR staining, single-cell suspensions were directly incubated with antibodies against FcγRs (FcγRI-BV605, Biolegend, #139323; FcγRII-APC,

Biolegend, #156406; FcγRIII-PE/Cy7, Biolegend, #158016; FcγRIV-BV421, Biolegend, #149521) without prior Fc blocking. After incubation, cells were stained with antibodies (CD45-RB705, BD Pharmingen, #570291 or CD45-BUV395, Biolegend, #103192; CD31-BV421, Biolegend, #102424; CD11b-APC/Cy7, Biolegend, #101225; F4/80-PE, Biolegend, #123110; Tim-4-PE/Cy7, Biolegend, #130010 or Tim-4-PerCP-eFluor™ 710, ThermoFisher, #46-5866-82; Ly6C-BV785, Biolegend, #128041; Ly6G-FITC, Biolegend, #127605; CD11c-BUV496, BD Pharmingen, #117348) in Brilliant Stain buffer (ThermoFisher, #00-4409-42) for the identification of cell populations and complement receptors (CRs). Viable cell populations were gated as Kupffer cells ($CD45^+CD31^-CD11b^{low}F4/80^{high}Tim\text{-}4^+$), macrophages ($CD45^+CD31^-CD11b^{low}F4/80^{high}$), monocytes ($CD45^+CD31^-CD11b^+ Ly6C^{high}Ly6G^-$), neutrophils ($CD45^+CD31^-CD11b^+Ly6G^{high}$), and endothelial cells ($CD45^-CD31^+$). All data were acquired on a CytoFLEX LX flow cytometer (Beckman Coulter) and analyzed with CytExpert software.

Bone marrow-derived macrophages (BMDMs)

Bone marrow-derived macrophages (BMDMs) were generated as follows. Bone marrow cells were isolated from the femurs and tibias of 6- to 8-week-old mice by flushing with ice-cold RPMI 1640 medium. The cell suspension was gently dissociated by pipetting, filtered through a 70-μm strainer, and treated with RBC lysis buffer. After washing, the cells were cultured for 7 days in RPMI 1640 medium supplemented with 10% endotoxin-free FBS (Sigma, F8318) and 30% L929-conditioned medium to induce macrophage differentiation. The L929-conditioned medium, serving as a source of M-CSF, was prepared by harvesting supernatant from L929 cells cultured for 5 days in DMEM with 10% FBS, followed by filtration through a 0.22-μm filter. After differentiation, BMDMs were subjected to one of the following treatments: infection with *S. aureus* or *E. coli* at the defined MOI (multiplicity of infection); stimulation with LPS (InvivoGen,

#tlrl-b5lps) or PGN (InvivoGen, #tlrl-pgns2) at the indicated concentrations; pretreatment with inhibitor, BAY11-7082 (Selleck, #S2913) for 1 hour in serum-free medium or fludarabine (TargetMol, #T1038) for 24 hours in medium containing 10% FBS, followed by stimulation with LPS or PGN. All treatments were performed for the indicated durations in medium containing 2% FBS. The identity of BMDMs was confirmed by flow cytometry, with >95% of the cells being $CD11b^{+}F4/80^{+}$. For intracellular FcRn detection, cells were then fixed, permeabilized, and stained with an EF647-conjugated anti-FcRn antibody (made in-house).

RNA extraction and qPCR analysis

Total RNA was isolated from tissue macrophages, BMDMs, or human umbilical vein endothelial cells (HUVECs) using TRIzol reagent (Invitrogen, #15596018CN) and reversely transcribed by StarScript III All-in-One gDNA Removal Mix (GenStar, #A230-10) according to the manufacturer's protocol. Quantitative PCR (qPCR) was performed with 2 × RealStar Green Fast Mixture (GenStar, #A301-10) and gene-specific primers (mouse *Fcgrt*: 5'-AGCTCAAGTTCCGATTCCTG-3' and 5'-GATCTGGCTGATGAATCTAGGTC-3'; human *Fcgrt*: 5'-GAAACCTGGAGTGGAAGGAG-3' and 5'-CGGAGGGTAGAAGGAGAAGG-3'; mouse *Tnf-α*: 5'-ATGAGAAGTTCCCAAATGGCC-3' and 5'-TCCACTTGGTGGTTTGCT ACG-3'; mouse *Ifn-β*: 5'-CCACCAGCAGACAGTGTTTC-3' and 5'-GAAGATCTCTGCTCGGACCA-3'; mouse *Ifn-γ*: 5'-TGAACGCTACACACTGCATCTTGG-3' and 5'-CGACTCCTTTTCCGCTTCCTGAG-3'). Relative mRNA levels were calculated via the 2^(-ΔΔCt) method with normalization to *Gapdh* (mouse: 5'-GAGAAACCTGCCAAGTATGATGAC-3' and 5'-ATCGAAGGTGGAAGAGTGGG-3'; human: 5'-CATCAAGAAGGTGGTGAAGCAG-3' and 5'-TTCATTGTCGTACCAGGAAATGAG-3').

Bulk RNA sequencing and analysis

Bulk RNA sequencing was performed on Kupffer cells and splenic macrophages. Kupffer cells were isolated by preparing a liver single-cell suspension from the liver, followed by direct fluorescence-activated cell sorting (FACS). Splenic macrophages were first enriched using anti-F4/80 magnetic beads (Stemcell, #100-0659) and subsequently purified by FACS to obtain a highly pure population. Cells were pooled from 3-7 mice for RNA extraction. Total RNA was extracted from the sorted cells using TRIzol reagent, and samples meeting quality thresholds (RIN/RQN $\geq$ 7.0; 28S/18S ratio $\geq$ 1.0) were selected for library construction. Sequencing was conducted on the DNBSEQ-T7 platform to generate 150 bp paired-end reads (PE150). For bioinformatic analysis, raw reads were processed with SOAPnuke to obtain high-quality clean data. Clean reads were then aligned to the mouse reference genome (GRCm39) using HISAT2. Gene expression levels were quantified with RSEM using the FPKM metric. Genes with a mean TPM > 0.5 across the group were considered expressed and retained for subsequent analysis. Differential expression analysis was performed using DESeq2, identifying genes with an absolute $\log_2$ fold change greater than 0.5 at a false discovery rate (FDR) of < 0.05 as statistically significant. Transcription factor (TF) activities were inferred from the shared differentially expressed genes using the decoupleR R package (v2.16.0) [48]. High-confidence mouse regulons (confidence levels A-C) were obtained from the DoRothEA database (v1.22.0) [49]. Sample-specific TF activity scores were estimated using the Univariate Linear Model (ULM) algorithm. For visualization, the top 20 TFs ranked by the mean absolute activity score across all samples are shown.

Western blotting

Whole-cell lysates were prepared from cells using RIPA lysis buffer supplemented with protease and phosphatase inhibitor cocktails (MedChemExpress, MCE). The lysates were denatured in 1× SDS loading buffer, separated by SDS-PAGE, and transferred onto polyvinylidene difluoride (PVDF) membranes. The membranes were blocked with QuickBlock™ blocking buffer (Beyotime, #P0252) and subsequently probed overnight at 4°C with the following primary antibodies: anti-phospho-STAT1 (Tyr701) (Abclonal, #AP0054), anti-phospho-STAT1 (Ser727) (Abclonal, #AP1000), anti-STAT1 (Abclonal, #A19563), and anti-β-actin (Abclonal, #AC050). After washing with TBST, the membranes were incubated with an HRP-conjugated goat anti-rabbit IgG (Jackson ImmunoResearch, #111-035-003) for 2 hours at room temperature. Protein bands were visualized using an Omni-ECL™ Ultra-Sensitive Chemiluminescence Detection Kit (Epizyme Biotech, #SQ201) and detected with a chemiluminescence imaging system.

ELISA for antibody binding

Binding measurements were performed in microtiter plates coated with 1×10^7 CFU of *S. aureus* Δ*spa*Δ*sbi*Δ*ssl10* or *E. coli* BSI099 bacteria in 0.1 M carbonate buffer (pH 9.5) at 4°C overnight or at 37°C for 2 hours. Wells were blocked by 2% (w/v) bovine serum albumin (BSA) before incubation with serial concentrations of test antibodies or indicated dilutions of mouse serum. Binding capacity was quantified following incubation with HRP-conjugated secondary antibodies.

Public dataset analysis

The prognostic value of FCGRT expression was assessed through analysis of public GEO datasets. The primary cohort, GSE65682 (n=478 with 28-day outcomes), was analyzed with the "maxstat" R package to determine an optimal cutoff for *Fcgrt* expression, thereby stratifying patients into high- and low-expression groups. Survival analysis was performed using Kaplan-Meier curves in

GraphPad Prism 10, with statistical significance determined by the log-rank test ($p < 0.05$). For independent validation, the GSE63042 cohort (n=106) was utilized, with patients dichotomized at the median *Fcgrt* expression level. Additionally, datasets GSE28750 and GSE33341 were integrated to compare *Fcgrt* expression levels between septic patients and healthy controls. To validate our experimental findings in human macrophages, we analyzed dataset GSE13670 focusing on *Fcgrt* expression at 8, 24, and 48 hours after *S. aureus* infection.

Isolation and differentiation of primary human monocytes (HMs)

Peripheral blood mononuclear cells (PBMCs) were isolated from the blood of healthy donors and septic patients by Ficoll density gradient centrifugation. $CD14^+$ monocytes were purified from PBMCs using magnetic microbeads (STEMCELL, #19359) according to the manufacturer's instructions. The monocytes were then differentiated into human monocyte-derived macrophages (hMDMs) by culturing for 7 days in RPMI-1640 medium supplemented with 10% FBS and 50 ng/mL human M-CSF (Biolegend, #574806) at 37°C with 5% CO_2. The medium was replaced every 3 days. For stimulation experiments, hMDMs or PBMCs were either treated with specified concentrations of LPS or PGN, or infected with bacteria at a defined MOI in medium containing 2% FBS; all treatments were carried out for the indicated durations. For inhibition, hMDMs were pretreated for 1 hour with either Ruxolitinib (RUX; 1 μM; MCE, #HY-50856) [50] or Adezmapimod (ADE/SB203580; 600 nM; MCE, #HY-10256)[51] to inhibit STAT1 phosphorylation at Tyr701 or Ser727, respectively. Subsequently, the cells were co-stimulated with LPS (1 μg/mL) and PGN (10 μg/mL) for 24 hours. For immunostaining, cells were first incubated with TruStain FcX™ (Biolegend, #422302) and a fixable viability dye (ThermoFisher, #eF506). Surface antigens were stained with CD11b-APC/Cy7 (Biolegend, #101225) and CD14-PE (Biolegend, #301805). Cells were then fixed, permeabilized, and stained intracellularly with antibodies against FcRn (EF647,

made in-house) and CD68-FITC (Biolegend, #333806). Viable monocytes ($CD11b^+CD14^+$) and macrophages ($CD11b^+CD14^+CD68^+$) were gated for flow cytometric analysis.

Antibody transcytosis assay

BMDMs and hMDMs were seeded in low-attachment 24-well plates at a density of 10^5 cells/well and treated with a PAMP (LPS, 1 μg/ml or PGN, 10 μg/ml) for 24 hours. After stimulation, medium was removed, and cells were then incubated with either FITC-dextran (100 μg/ml) or Alexa Fluor 647-labeled hIgG1(5 μg/ml) diluted in fresh medium containing the respective PAMP for indicated durations. Following incubation, cells were washed twice with PBS containing 0.1% BSA and resuspended in a residual volume of 50 μl. An equal volume of IC fixation buffer (ThermoFisher, #88-8824-00) was added for fixation at room temperature for 30 mins. Cells were washed once with 0.01% BSA-PBS and resuspended for flow cytometry [52,53].

Evaluation of antibody protection in mice

The efficacy of IVIG and 3E9 mAb was evaluated in a monomicrobial murine sepsis model. Mice received an intraperitoneal injection of the indicated antibody dose 12-16 hours before bacterial challenge. The STAT1 inhibitor carnosic acid (CA) was administered *via* intraperitoneal injection. The inhibitor was given at a dose of 20 mg/kg, dissolved in a solution (5 % DMSO, 30 % PEG300, 10 % tween 80, 55 % H_2O), twice daily for 3 days, with the initial dose administered 2 hours prior to bacterial challenge. Under anesthesia, mice were inoculated via the retro-orbital venous plexus with 100 μl of a bacterial suspension in PBS at a concentration of 5×10^8 CFU/ml (*S. aureus* Δ*spa*Δ*sbi*Δ*ssl10*) or 3×10^9 CFU/ml (*E. coli* BSI099). Following infection, survival was monitored 2 to 3 times daily.

Statistical analysis

Data are presented as mean ± SEM. For comparisons between two groups, an unpaired, two-tailed Student's *t* test was applied. When three or more groups were compared under a single independent variable, a one-way ANOVA with multiple comparisons test was conducted. To assess the effects of two independent variables, data were analyzed by two-way ANOVA with multiple comparisons test. Mouse survival was statistically compared using the log-rank (Mantel-Cox) test. All data were analyzed by Prism 10 (GraphPad Software), and statistical significance was indicated as follows: *, $P < 0.05$; **, $P < 0.01$; ***, $P < 0.001$.

Methods references

43 Wang, J. *et al.* Liver macrophages and sinusoidal endothelial cells execute vaccine-elicited capture of invasive bacteria. *Science translational medicine* **15**, eade0054 (2023).

44 Kim, H. K., Cheng, A. G., Kim, H.-Y., Missiakas, D. M. & Schneewind, O. Nontoxigenic protein A vaccine for methicillin-resistant Staphylococcus aureus infections in mice. *Journal of Experimental Medicine* **207**, 1863–1870 (2010). https://doi.org/10.1084/jem.20092514

45 Chen, X. *et al.* Glycosylation-dependent opsonophagocytic activity of staphylococcal protein A antibodies. *Proceedings of the National Academy of Sciences* **117**, 22992–23000 (2020). https://doi.org/10.1073/pnas.2003621117

46 Blumberg, L. *et al.* Blocking FcRn in humans reduces circulating IgG levels and inhibits IgG immune complex–mediated immune responses. *Science advances* **5**, eaax9586 (2019).

47 An, H., Tian, X., Huang, Y. & Zhang, J.-R. Identification of the mouse Kupffer cell receptors recognizing pneumococcal capsules by affinity screening. *STAR Protocols* **4** (2023). https://doi.org/10.1016/j.xpro.2023.102065

48 Badia-i-Mompel, P. *et al.* decoupleR: ensemble of computational methods to infer biological activities from omics data. *Bioinformatics advances* **2**, vbac016 (2022).

49 Holland, C. H., Szalai, B. & Saez-Rodriguez, J. Transfer of regulatory knowledge from human to mouse for functional genomics analysis. *Biochimica et Biophysica Acta (BBA)-Gene Regulatory Mechanisms* **1863**, 194431 (2020).

50 Hashimoto, R., Koide, H. & Katoh, Y. MEK inhibitors increase the mortality rate in mice with LPS-induced inflammation through IL-12-NO signaling. *Cell Death Discovery* **9** (2023). https://doi.org/10.1038/s41420-023-01674-w

51 Shi, Q. *et al.* The p38 MAPK inhibitor SB203580 differentially modulates LPS-induced interleukin 6 expression in macrophages. *Central European Journal of Immunology* **40**, 276–282 (2015). https://doi.org/10.5114/ceji.2015.54586

52 Yu, L. *et al.* FcRn-dependent IgG accumulation in adipose tissue unmasks obesity pathophysiology. *Cell Metabolism* **37**, 656–672.e657 (2025). https://doi.org/10.1016/j.cmet.2024.11.001

53 Toh, W. H. *et al.* FcRn mediates fast recycling of endocytosed albumin and IgG from early macropinosomes in primary macrophages. *Journal of Cell Science* **133** (2020). https://doi.org/10.1242/jcs.235416

Acknowledgments: We thank the Biosafety Level 2 (BSL-2) and Animal Biosafety Level 2 (ABSL-2) Laboratories of the Institute of Infectious Diseases, Shenzhen Bay Laboratory, for their support and assistance during this research. This study was supported by the National Natural Science Foundation of China: 32571106 (X.C.), the National Natural Science Foundation of China: 82371836 (X.C.), the Guangdong Pearl River Funding: 2023QN10Y181 (X.C.), the Start-up funding from Shenzhen Bay Laboratory (X.C.), the National Natural Science Foundation of China: 82501943 (W.C), and the GuangDong Basic and Applied Basic Research Foundation: 2023A1515111092 (W.C).

Author contributions:

Conceptualization: X.C., X.W., X.S., and Q.D.; Methodology: X.W., X.S., M.P., Q.D., Q.H., X.L., J.Z., D.W., B.C., Y.D., Y.H., J.Y., and T.Z.; Validation: X.C., X.W., X.S., and Q.D.; Investigation: X.S. and X.W.; Resources: W.C., X.L., H.Z., X.H., M.L., and X.D.; Visualization: X.C., X.W., X.S., and Q.D.; Funding acquisition: X.C., and W.C.; Project administration: X.C., W.C., and X.L.; Supervision: X.C.; Writing – original draft: X.C., X.W., and X.S.; Writing – review & editing: X.C., W.C., and X.L.

Competing interests: Authors declare that they have no competing interests.

Data and materials availability: The raw sequence data reported in this paper have been deposited in the Genome Sequence Archive (Genomics, Proteomics & Bioinformatics 2025) in National Genomics Data Center (Nucleic Acids Res 2025), China National Center for Bioinformation / Beijing Institute of Genomics, Chinese Academy of Sciences (GSA: CRA036603) that are publicly accessible at https://ngdc.cncb.ac.cn/gsa.

Additional information

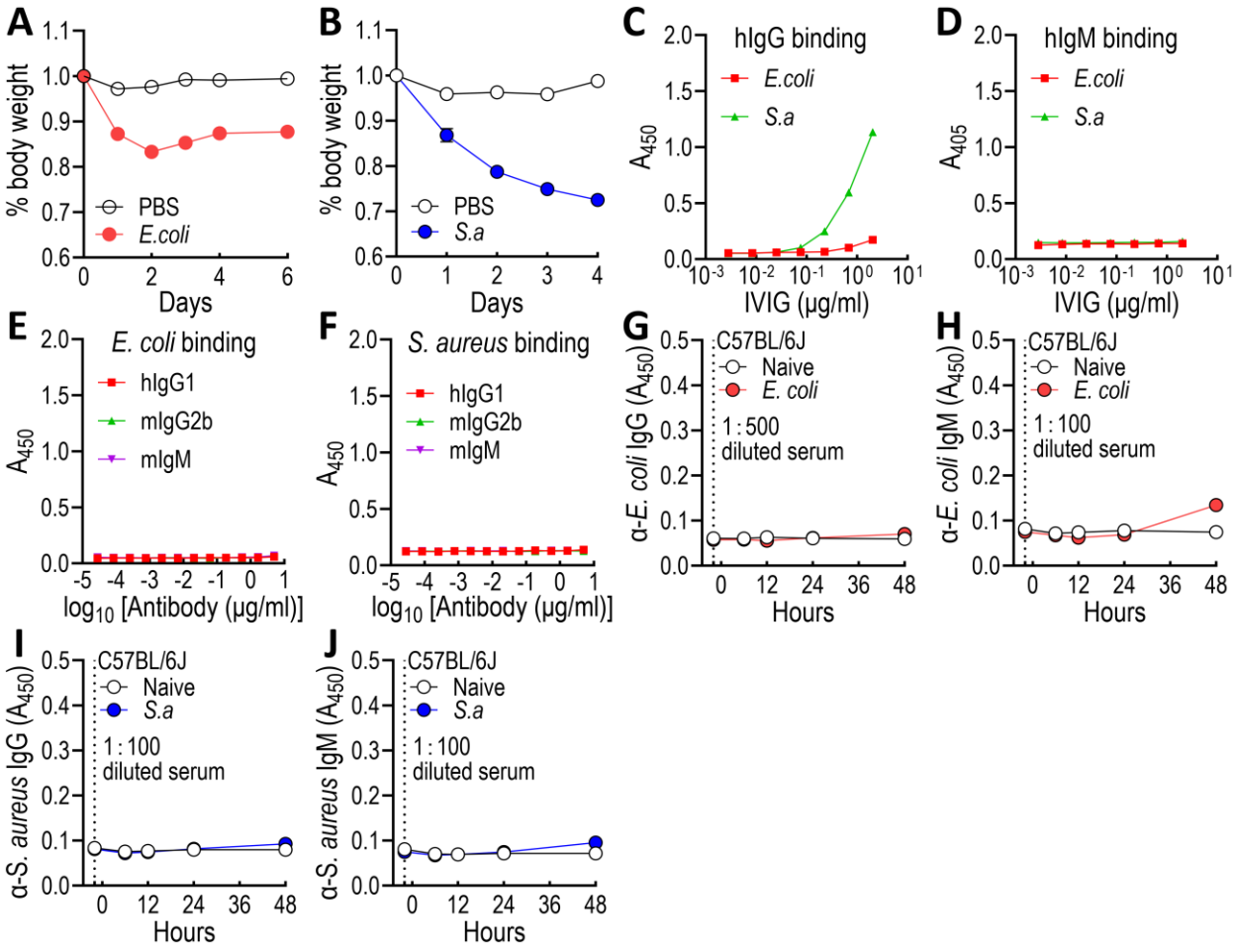

Extended Figure 1.

Loss of endogenous and exogenous IgG in septic mice. (A and B) Relative body weight in C57BL/6J mice (n = 6) with pathogenic *E. coli*- (A) or *S. aureus* Δ*spa*Δ*sbi*Δ*ssl10* (B)-induced sepsis. (C and D) ELISA analysis (n = 3) of IVIG binding to *E. coli* or *S. aureus* Δ*spa*Δ*sbi*Δ*ssl10*, detecting bound hIgG (C) and hIgM (D). (E and F) ELISA analysis (n = 3) of hIgG1, mIgG2b, and mIgM mAb binding to *E. coli* (E) or *S. aureus* Δ*spa*Δ*sbi*Δ*ssl10* (F). (G to J) Detection of serum IgG (G and I) and IgM (H and J) antibodies against *E. coli* (G and H) or *S. aureus* Δ*spa*Δ*sbi*Δ*ssl10* (I and J) in mice (n = 5) at indicated times after septic challenge with respective bacterium. Data are presented as mean ± SEM.

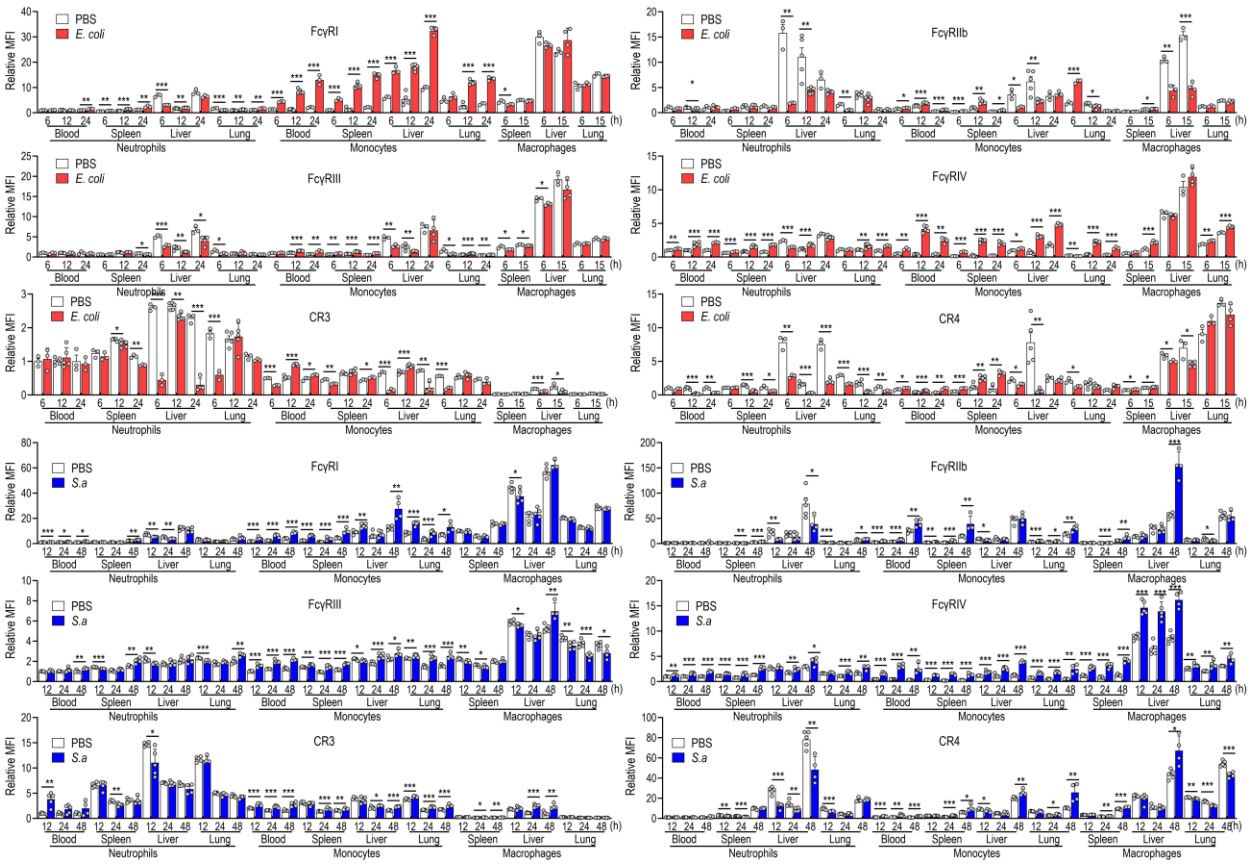

Extended Figure 2.

Expression of FcγR and complement receptor (CR) in immune cells from septic mice. Four FcγRs (FcγRI, FcγRIIb, FcγRIII, and FcγRIV) and two CRs (CR3 and CR4) were quantified in neutrophils, monocytes, and macrophages from blood and different tissues by flow cytometry analysis. The blood and tissue samples were collected from C57BL/6J mice (n = 3 to 5) challenged with PBS, pathogenic *E. coli*, or *S. aureus* Δ*spa*Δ*sbi*Δ*ssl10*. Data are presented as mean ± SEM. Significant differences (*p < 0.05, **p < 0.01, and ***p < 0.001) were identified by two-tailed Student's *t* test.

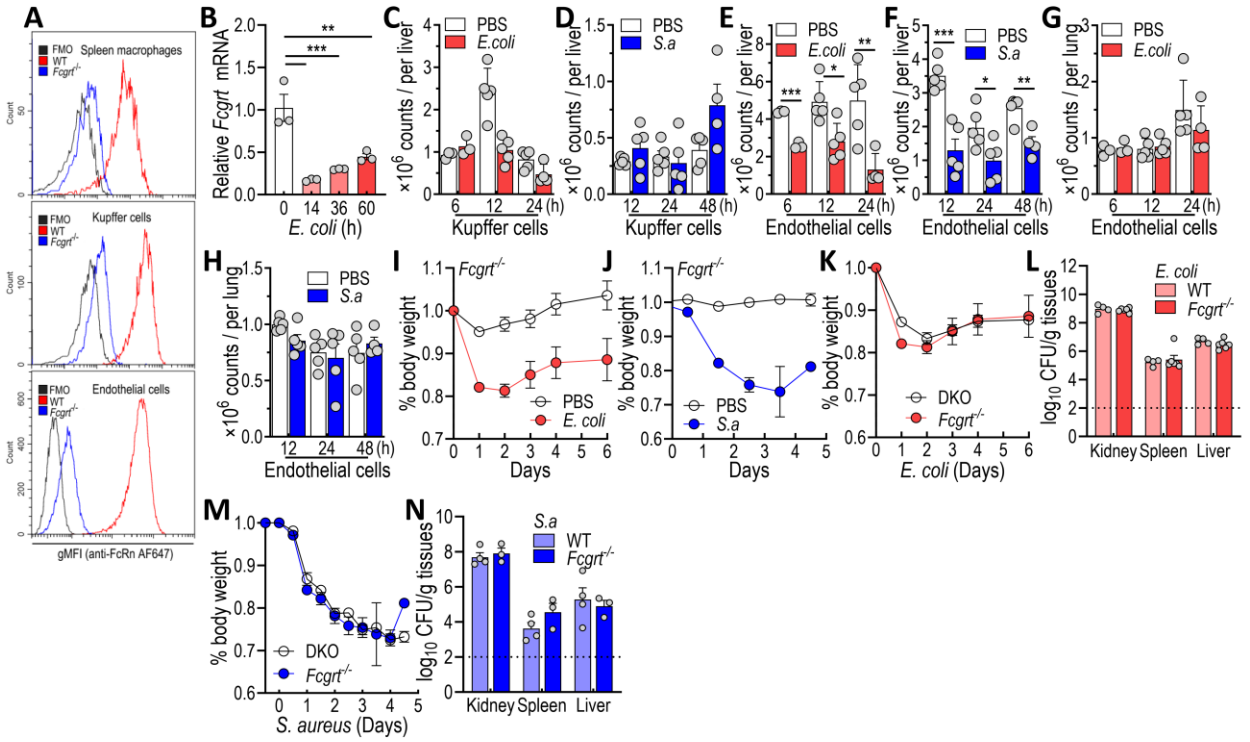

Extended Figure 3.

Macrophage FcRn reduction-mediated loss of circulating IgG in septic mice. (A) Confirmation of specificity of anti-FcRn mAb in tissue macrophages from WT and *Fcgrt*$^{-/-}$ mice by flow cytometry analysis. (B) qPCR analysis of *Fcgrt* expression in splenic macrophages (n = 3) isolated from mice during sepsis induced by *E. coli*. (C to H) The numbers of Kupffer cells (C and D), liver endothelial cells (E and F), and lung endothelial cells (G and H) in mice (n = 3 to 5) after septic challenge with *E. coli* or *S. aureus* Δ*spa*Δ*sbi*Δ*ssl10*. (I and J) Relative body weight in *Fcgrt*$^{-/-}$ C57BL/6J mice (n = 3 to 5) with pathogenic *E. coli*- (I) or *S. aureus* Δ*spa*Δ*sbi*Δ*ssl10* (J)-induced sepsis. (K and M) Comparison of relative body weight between DKO (n = 5) and *Fcgrt*$^{-/-}$ (n = 6) mice after septic challenge with *E. coli* (K) or *S. aureus* Δ*spa*Δ*sbi*Δ*ssl10* (M). (L and N) Comparison of bacterial loads in tissues between DKO and *Fcgrt*$^{-/-}$ mice (n = 4 to 6) at 96 hours after septic challenge with *E. coli* (L) or *S. aureus* Δ*spa*Δ*sbi*Δ*ssl10* (N). Data are presented as mean

± SEM. Significant differences (*p < 0.05, **p < 0.01, and ***p < 0.001) were identified in B by one-way ANOVA analysis.

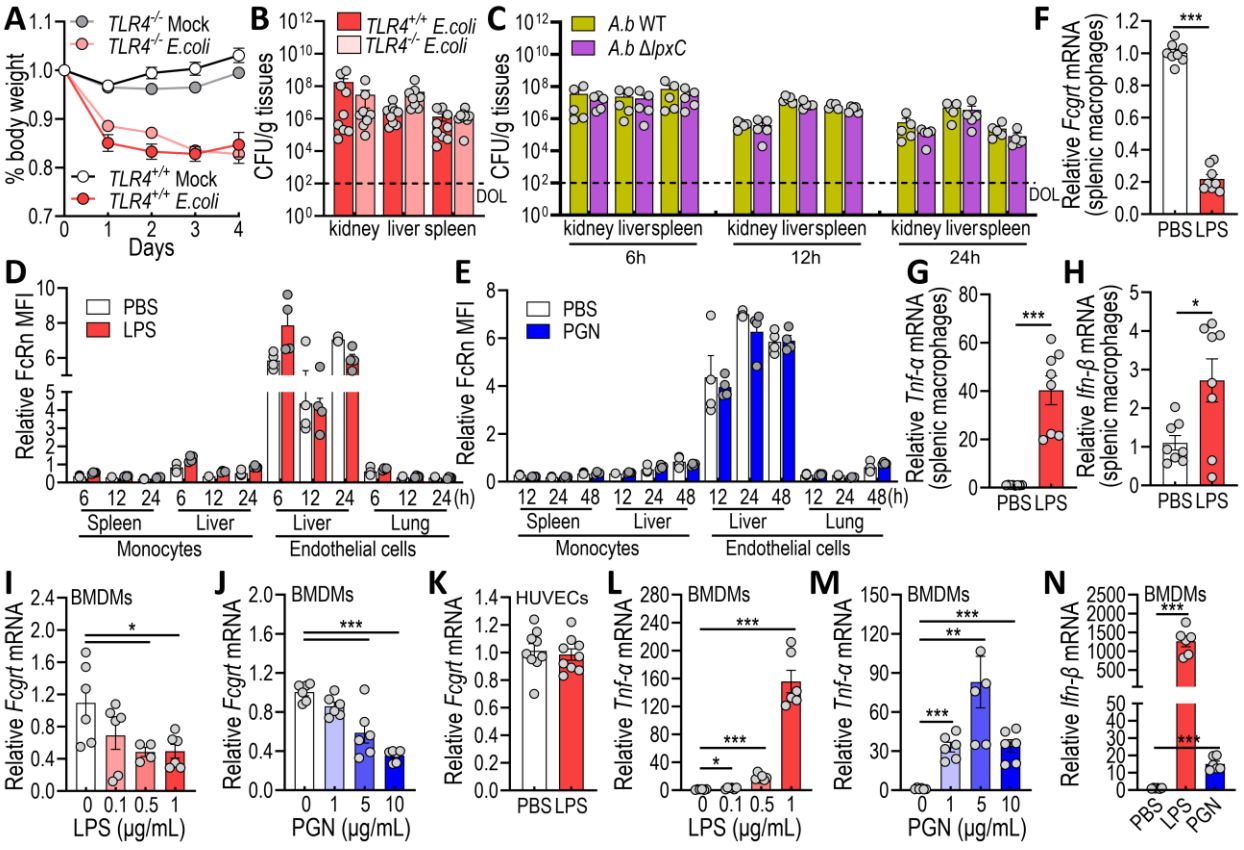

Extended Figure 4.

Bacteria-derived PAMPs as a cause of sepsis-associated IgG loss in mice. (A) Relative body weight in *TLR4*$^{+/+}$ and *TLR4*$^{-/-}$ C57BL/6J mice (n = 10) with pathogenic *E. coli*-induced sepsis. (B) Bacterial loads in tissues from *TLR4*$^{+/+}$ and *TLR4*$^{-/-}$ C57BL/6J mice at 96 hours after septic challenge with pathogenic *E. coli*. (C) Bacterial loads in tissues from mice at indicated times after septic challenge with *A. baumannii* WT or Δ*lpxC*. (D and E) Flow cytometry analysis of relative FcRn expression in monocytes and endothelial cells isolated from murine tissues (n = 3 to 5) at indicated times after LPS (D, 5 mg/kg) or PGN (E, 10 mg/kg) challenge. (F to H) qPCR analysis

of *Fcgrt* (F), *Tnf-α* (G), and *Ifn-β* (H) expression in splenic macrophages from PBS- or LPS-treated C57BL/6J mice ($n = 8$). (I and J) qPCR analysis of *Fcgrt* expression in BMDMs ($n = 5$ to 6) treated with indicated doses of LPS (I) or PGN (J) for 6 h. (K) qPCR analysis of *Fcgrt* expression in HUVECs ($n = 9$) treated with LPS (1 μg/ml) for 12h. (L to N) qPCR analysis of *Tnf-α* (L and M) and *Ifn-β* (N) expression in BMDMs ($n = 5$ to 6) treated with indicated doses of LPS or PGN for 6 h. Data are presented as mean ± SEM. Significant differences (*$p < 0.05$, **$p < 0.01$, and ***$p < 0.001$) were identified in F-H by two-tailed Student's *t* test and in I, J, L, M, and N by one-way ANOVA analysis.

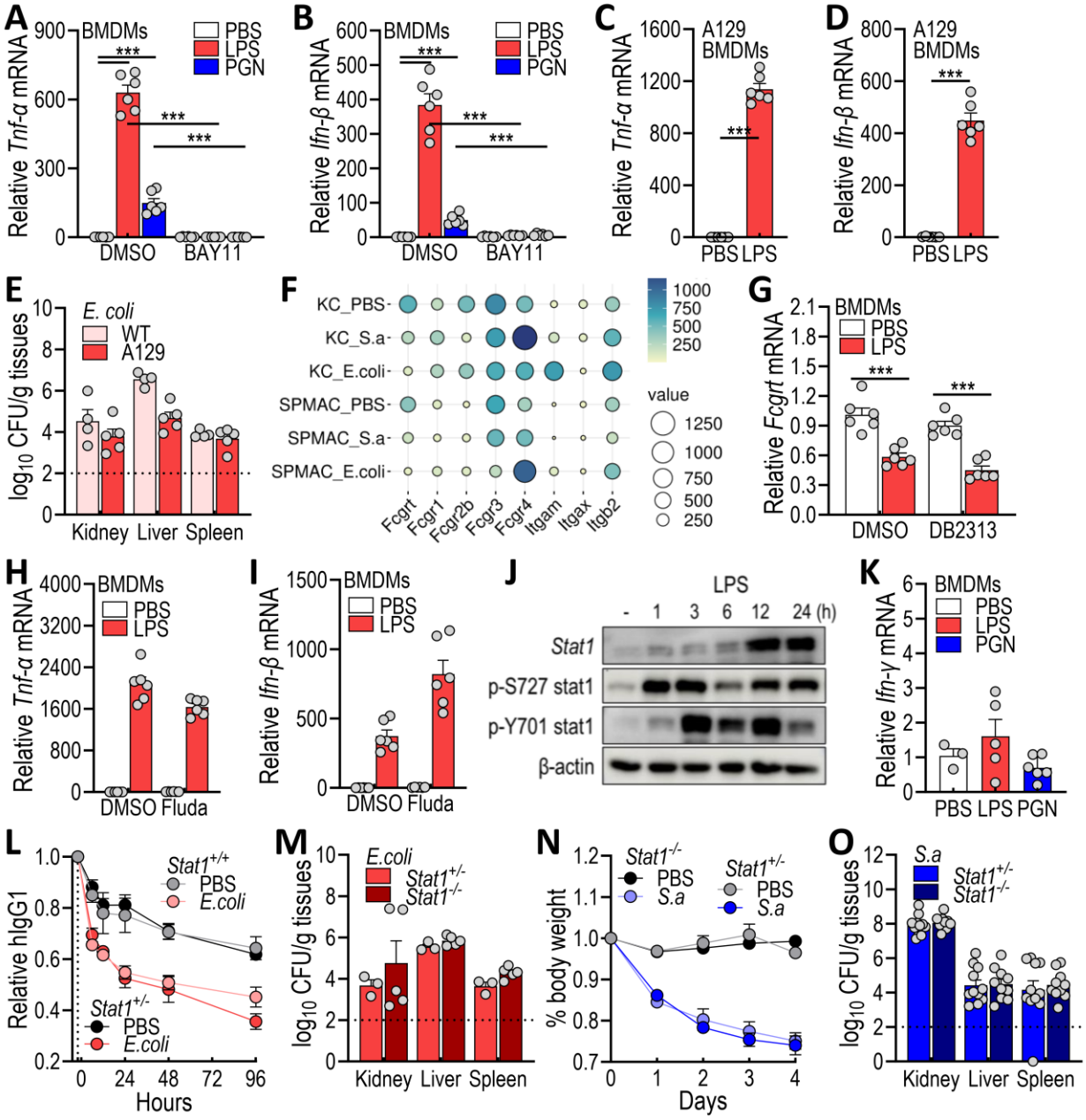

Extended Figure 5.

STAT1 activation-mediated FcRn reduction and IgG loss in septic mice. (A and B) Effect of NF-κB inhibitor BAY11-7082 (BAY11, 10 μM) on *Tnf-α* (A) and *Ifn-β* (B) expression in BMDMs (n = 6) treated with LPS (1 μg/ml) or PGN (10 μg/ml) for 12h. (C and D) qPCR analysis of *Tnf-α* (C) and *Ifn-β* (D) expression in A129 mouse-derived BMDMs (n = 6) treated with LPS (1 μg/ml)

for 12h. (E) Bacterial loads in tissues from A129 mice at 96 hours after septic challenge with pathogenic *E. coli*. (F) Expression levels of FcRn, FcγRs, and CRs in kupffer cells (KC) and splenic macrophages (SPMAC) from septic mice. Transcriptomic data were derived from mice with sepsis induced by pathogenic *E. coli* or *S. aureus* Δ*spa*Δ*sbi*Δ*ssl10*. (G) qPCR analysis of *Fcgrt* expression in BMDMs (n = 6) treated with PU.1 (encoded by the *Spi1* gene) inhibitor DB2313 (300 nM) and stimulated with LPS (1 μg/ml) for 12h. (H and I) Effect of STAT1 inhibitor Fludarabine (Fluda, 50 μM) on *Tnf-α* (H) and *Ifn-β* (I) expression in BMDMs (n = 6) treated with LPS (1 μg/ml) for 12h. (J) Western blotting analysis of STAT1 phosphorylation in BMDMs treated with 1 μg/ml LPS. β-actin was used as the loading control. (K) qPCR analysis of *Ifn-γ* expression in BMDMs (n = 3 to 6) treated with LPS (1 μg/ml) or PGN (10 μg/ml) for 12h. (L) Serum hIgG1 kinetics in *Stat1*$^{+/-}$ and *Stat1*$^{+/+}$ C57BL/6J mice (n = 5) following its administration and subsequent septic challenge with pathogenic *E. coli*. (M and O) Bacterial loads in tissues from *Stat1*$^{+/-}$ and *Stat1*$^{-/-}$ C57BL/6J mice at 96 hours after septic challenge with *E. coli* (M, n = 3 to 5) or *S. aureus* Δ*spa*Δ*sbi*Δ*ssl10* (O, n = 11). (N) Relative body weight in *Stat1*$^{+/-}$ and *Stat1*$^{-/-}$ C57BL/6J mice (n = 10) with pathogenic *S. aureus* Δ*spa*Δ*sbi*Δ*ssl10*-induced sepsis. Data are presented as mean ± SEM. Significant differences (*p < 0.05, **p < 0.01, and ***p < 0.001) were identified in A, B, and G by one-way ANOVA analysis and in C and D by two-tailed Student's t test.

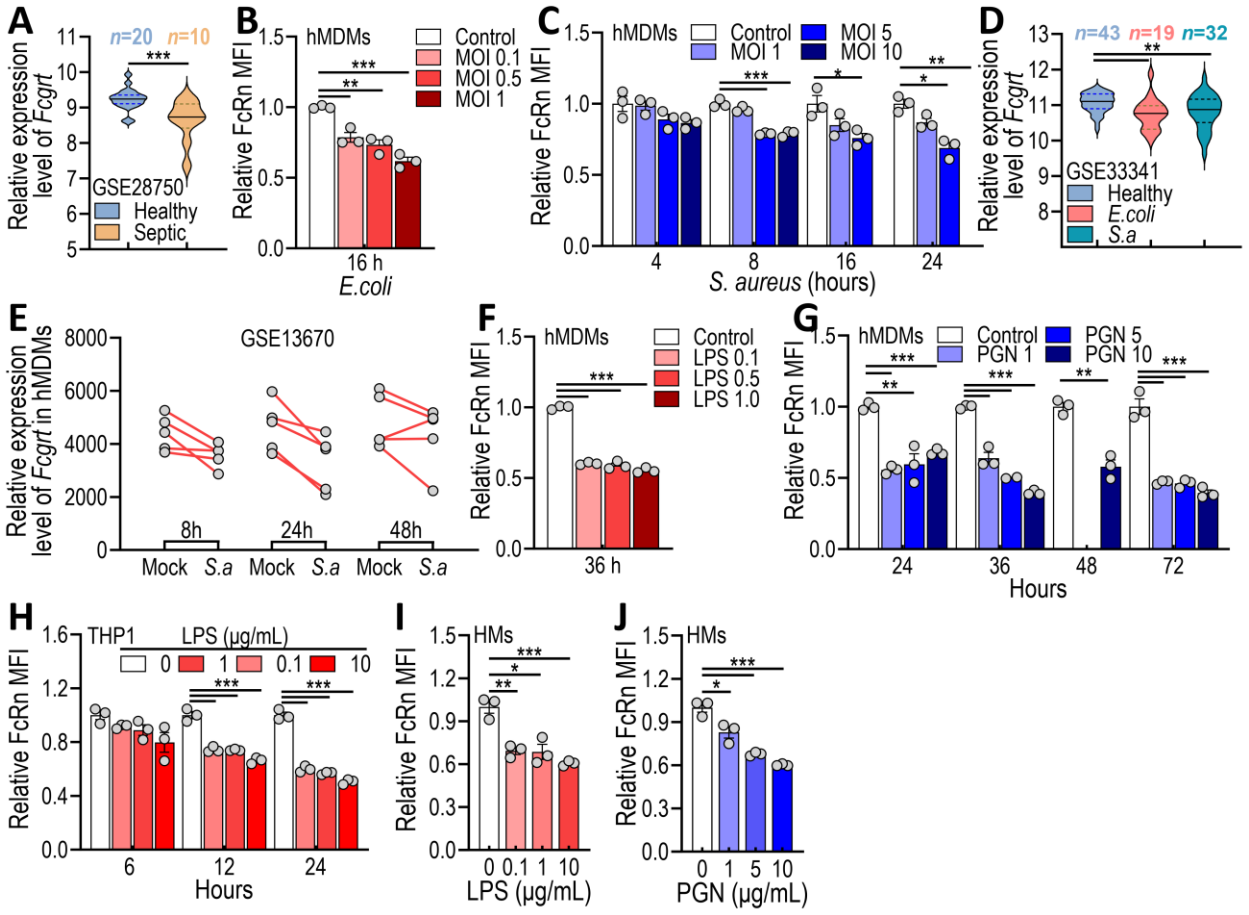

Extended Figure 6.

Conservation of the bacteria-PAMP-STAT1 pathway driving FcRn reduction in humans. (A) Analysis of *Fcgrt* expression in a public dataset (GSE28750) of whole-blood leukocytes from healthy donors and septic patients. (B and C) Flow cytometry analysis of FcRn expression in hMDMs (n = 3) infected with *E. coli* (B) or *S. aureus* Δ*spa*Δ*sbi*Δ*ssl10* (C) at indicated MOIs and times. (D) Analysis of *Fcgrt* expression in a public dataset (GSE28750) of whole-blood leukocytes from healthy donors and septic patients with infections caused by *E. coli* or *S. aureus*. (E) Analysis of *Fcgrt* expression in a public dataset (GSE13670), featuring hMDMs infected with *S. aureus* at indicated times. (F and G) Flow cytometry analysis of FcRn expression in hMDMs (n = 3) stimulated with LPS (F) or PGN (G) at indicated concentrations and times. (H to J) Flow cytometry

analysis of FcRn expression in THP1 cells (H, n = 3) and human CD14+ monocytes (I and J, n = 3) stimulated with LPS (H, I) or PGN (J) at indicated concentrations and times. Data are presented as mean ± SEM. Significant differences (*p < 0.05, **p < 0.01, and ***p < 0.001) were identified in A by two-tailed Student's t test and in B, C, D, F, G, H, I, and J by one-way ANOVA analysis.

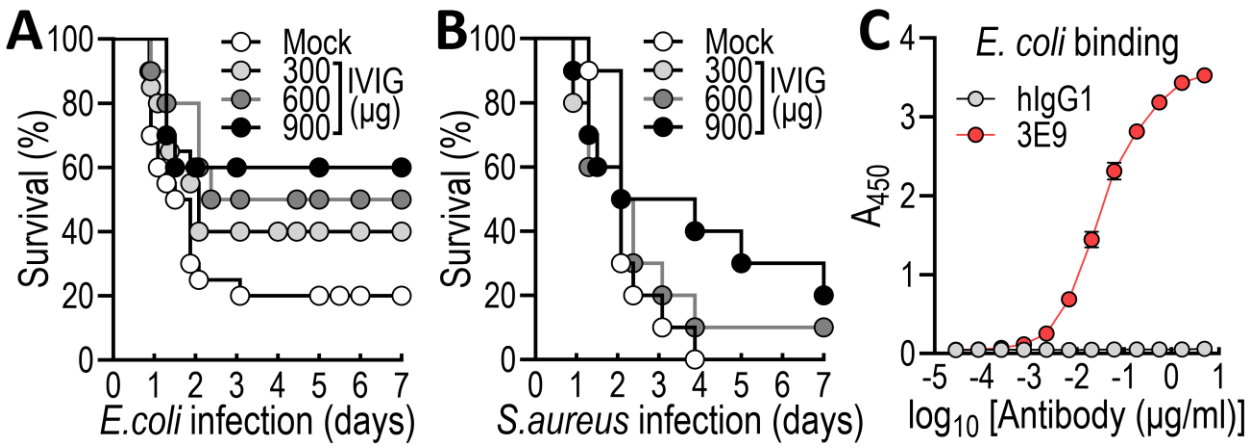

Extended Figure 7.

Antibody efficacy in mice with bacterial sepsis. (A and B) Survival of mice (n = 10) after IVIG administration at indicated doses, followed by septic challenge with *E. coli* (A) or *S. aureus* Δ*spa*Δ*sbi*Δ*ssl10* (B). (C) ELISA analysis (n = 3) of hIgG1 and 3E9 mAb binding to *E. coli*. Data are presented as mean ± SEM.